A Novel Dimanganese(III) Complex with a Single Hydroxo Bridge. Syntheses, Structures, and Magnetic Susceptibilities of (μ-Hydroxo)bis((octaethylporphinato)manganese(III)) Perchlorate and a Monomeric Precursor, Aquo(octaethylporphinato)manganese(III) Perchlorate

Beisong Cheng,[1a] Fabio Cukiernik,[1b] Pascal H. Fries,*[,1b] Jean-Claude Marchon,*[,1b] and W. Robert Scheidt*[,1a]

Department of Chemistry and Biochemistry, University of Notre Dame, Notre Dame, Indiana 46556, and CEA/Département de Recherche Fondamentale sur la Matière Condensée/SESAM and CNRS/Laboratoire de Chimie de Coordination (Unité de Recherche Associée No. 1194), Centre d'Études Nucléaires de Grenoble, 38054 Grenoble Cedex, France

Received June 1, 1995[⊗]

The synthesis and structural and magnetic characterization of a dimanganese(III) complex with a novel, single, hydroxo bridge is described. The complex, (μ-hydroxo)bis((octaethylporphinato)manganese(III)) perchlorate, can be prepared by protonation of an oxo-bridged manganese complex or, more reliably, by hydrolysis of monomeric manganese(III) octaethylporphyrinates. The crystal and molecular structure has been solved using X-ray diffraction data collected with an area detector. The two five-coordinate manganese(III) ions in $\{[Mn(OEP)]_2(OH)\}ClO_4$ are bridged by a single hydroxo ligand with an average Mn−O distance of 2.011 Å and a Mn−O(H)−Mn bridge angle of 152.73°. The average $Mn-N_p$ distance is 2.006 Å. The two porphyrin rings are crowded against each other and are hence canted with a dihedral angle of 12.7°. An additional distortion from ring crowding occurs in the coordination angles $O-Mn-N_p$ at one manganese(III) ion but not at the other. The magnetic susceptibility of the hydroxo-bridged complex has been measured over the temperature range 2−300 K. The observed behavior is typical of an exchange-coupled binuclear complex. The data have been fit to the total spin Hamiltonian ($\mathcal{H}_{tot} = \mathcal{H}(1) + \mathcal{H}(2) - 2J\tilde{S}_1\cdot\tilde{S}_2$) of a zero-field-split, high-spin d^4-d^4 dimer in its actual crystallographic geometry, using numerical techniques. The hydroxide bridge supports a relatively strong antiferromagnetic coupling ($2J = -71.0 \pm 0.4$ cm^{-1}) between two zero-field-split ($D = -8 \pm 2$ cm^{-1}) manganese(III) ions. The synthesis and characterization of one monomeric precursor, $[Mn(OEP)(H_2O)]ClO_4\cdot H_2O$, is also reported. This species is a simple paramagnet. The crystal structure analysis shows it to be a five-coordinate, high-spin manganese(III) complex. Crystal data: $\{[Mn(OEP)]_2(OH)\}ClO_4\cdot 3CH_2Cl_2$, $a = 14.791(4)$ Å, $b = 14.895(2)$ Å, $c = 18.634(4)$ Å, $\alpha = 69.79(2)°$, $\beta = 89.24(2)°$, $\gamma = 88.86(2)°$, triclinic, space group $P\bar{1}$, $V = 3851.7(14)$ Å^3, $Z = 2$, $R_1 = 0.0655$ for 15 643 observed data based on $F_o \geq 4.0\sigma(F_o)$, $wR_2 = 0.1631$ for 19 422 total unique data, least-squares refinement on F^2 using all data; $[Mn(OEP)(H_2O)]ClO_4\cdot H_2O$, $a = 12.800(1)$ Å, $b = 13.506(4)$ Å, $c = 13.355(7)$ Å, $\alpha = 64.80\ (2)°$, $\beta = 62.36(3)°$, $\gamma = 85.67(3)°$, triclinic, space group $P\bar{1}$, $V = 1829.1(11)$ Å^3, $Z = 2$, $R_1 = 0.0754$ for 5715 observed data based on $F_o \geq 4.0\sigma(F_o)$, $wR_2 = 0.2210$ for 8891 total unique data, least-squares refinement on F^2 using all data.

Introduction

Multinuclear manganese species are an essential component in a number of metalloenzymes.[2−5] Dimanganese systems are important in the redox enzymes catalase[6] and pseudocatalase[7] and a ribonucleotide reductase.[8] The most celebrated manganese-containing system is that of photosystem II (PS II)[9] for water splitting and dioxygen evolution, which is thought to be a tetranuclear system. Although direct evidence for the identity of the bridging ligands is limited, the relatively small Mn···Mn distances (EXAFS,[10] 2.7−3.6 Å), electron paramagnetic resonance spectra, electronic spectra and magnetic susceptibility measurements, and the analogy to a number of similar diiron systems suggest that the manganese atoms are linked by oxo

[⊗] Abstract published in *Advance ACS Abstracts,* August 1, 1995.

(1) (a) University of Notre Dame. (b) Centre d'Etudes Nucléaires de Grenoble.
(2) *Manganese Redox Enzymes*; Pecoraro, V. L., Ed.; VCH: New York, 1992.
(3) Que, L., Jr.; True, A. E. In *Progress in Inorganic Chemistry: Bioinorganic Chemistry*; Lippard, S. J., Ed.; Interscience: New York, 1990; Vol. 38, Chapter 3.
(4) Wieghardt, K. *Angew. Chem., Int. Ed. Engl.* **1989**, *28*, 1153.
(5) Brudvig, G. W. In *Metal Clusters in Proteins*; Que, L., Jr., Ed.; ACS Symposium Series 372; American Chemical Society: Washington, DC, 1988; pp 221−237. Christou, G.; Vincent, J. B. In *Metal Clusters in Proteins*; Que, L., Jr., Ed.; ACS Symposium Series 372; American Chemical Society: Washington, DC, 1988; pp 238−255.
(6) Vainshtein, B. K.; Melik-Adamyan, V. R.; Barynin, V. V. *Kristallografia* **1981**, *26*, 10003. Vainshtein, B. K.; Melik-Adamyan, V. R.; Barynin, V. V.; Vagin, A. A.; Grebenko, A. I. *J. Biosci. (Bangalore, India), Suppl.* **1985**, *8*, 471.
(7) Kono, Y.; Fridovich, I. *J. Biol. Chem.* **1983**, *258*, 6015. Kono, Y.; Fridovich, I. *J. Biol. Chem.* **1983**, *258*, 13646. Beyer, W. F., Jr.; Fridovich, I. *Biochemistry* **1985**, *24*, 6460.
(8) Willing, A.; Follmann, H.; Auling, G. *Eur. J. Biochem.* **1988**, *170*, 603. Plonzig, J.; Auling, G. *Arch. Microbiol.* **1987**, *146*, 396. Follmann, H.; Willing, A.; Auling, G.; Plonzig, J. In *Thioredoxin and Glutaredoxin Systems: Structure and Function*; Holmgren, A., et al., Eds.; Raven Press: New York, 1986.
(9) Selected references: Dismukes, G. C. *Photochem. Photobiol.* **1986**, *43*, 99. dePaula, J. C.; Brudvig, G. W. *J. Am. Chem. Soc.* **1985**, *107*, 2643. Kirby, J. A.; Robertson, A. S.; Smith, J. P.; Thompson, A. C.; Cooper, S. R.; Klein, M. P. *J. Am. Chem. Soc.* **1981**, *103*, 5529.
(10) OEP, TPP, and Pc = the dianions of octaethylporphyrin, tetraphenylporphyrin, and phthalocyanine, respectively; Py = pyridine; DMF = dimethylformamide; EXAFS = extended X-ray absorption fine structure; $[Mn_2O(5\text{-}NO_2saldien)_2]$ = the Schiff base 1,7-bis((5-nitrosalicylidene)amino)-3-azapentane.

0020-1669/95/1334-4627$09.00/0

and/or hydroxo groups, together with other bridging ligands such as carboxylates. In such bridged systems, the protonation and deprotonation of the oxo bridge may be important in the catalytic cycle of these redox enzymes. Recently, Naruta et al.[11] reported that a binuclear Mn(III) porphyrin complex can lead to oxygen evolution from water. An essential feature of their proposed mechanism is the formation of hydroxide complexes of the porphyrin dimer. The electronic structure and the interaction between manganese centers are thus of some considerable interest, and the synthesis and characterization of manganese complexes with well-defined and simple bridging ligand systems seem to be especially so.

We recently communicated the synthesis and characterization of the first example of a singly hydroxo-bridged diiron(III) complex, the iron(III) porphyrinate derivative $\{[Fe(OEP)]_2(OH)\}ClO_4$,[12] which was prepared by the protonation of the oxo-bridged complex $[Fe(OEP)]_2O$. Our preliminary magnetic measurements on the iron system suggested a significant antiferromagnetic coupling mediated by the μ-hydroxo bridge. We have continued our studies of this novel μ-hydroxo bridging system with the preparation and characterization of the analogous manganese complex $\{[Mn(OEP)]_2(OH)\}ClO_4$. Protonation of the oxo-bridged species did yield the desired μ-hydroxo complex, but the reaction was marred by difficulties of consistency. Our reported synthesis of the μ-hydroxo−dimanganese species makes use of monomeric starting materials, is straightforward and reproducible, and does not necessarily proceed through an oxo-bridged intermediate. $\{[Mn(OEP)]_2(OH)\}ClO_4$ appears to be the first case of a dimanganese compound bridged by a single hydroxo bridge, as was the case with the analogous iron complex. Herein, we report the detailed synthesis, X-ray structure, and temperature-dependent magnetic susceptibility characterization of hydroxo-bridged $\{[Mn(OEP)]_2(OH)\}ClO_4$ and $[Mn(OEP)(H_2O)]ClO_4$, a monomeric precursor. The bridging hydroxide ligand is found to mediate a relatively strong antiferromagnetic interaction between the two manganese(III) centers of the dinuclear species. The mononuclear complex $[Mn(OEP)(H_2O)]ClO_4\cdot H_2O$ is found to be a simple paramagnetic species.

Experimental Section

General Information. H_2OEP was purchased from Midcentury Chemicals, and manganese acetate from Alfa; $HClO_4$ and $CDCl_3$ (99.8 atom % D) were purchased from Aldrich, and all other reagents were obtained from Fisher. All these materials were used as received unless otherwise noted. Coaxial NMR tubes for solution magnetic susceptibility measurements were bought from Wilmad Glass. IR spectra were recorded on a Perkin-Elmer 883 infrared spectrophotometer as CsBr pellets; electronic spectra were recorded on a Perkin-Elmer Lambda 19 UV/vis/near-IR spectrometer, and NMR spectra were recorded on a General Electric GN300 spectrometer.

Synthetic Procedures. [Mn(OEP)Cl]. A modified Adler synthesis[13] was used to prepare [Mn(OEP)Cl]. H_2OEP (1 g) was reacted with 5 g of finely divided $Mn(OAc)_2$ in 300 mL of refluxing DMF for 2 h. The reaction system was cooled and extracted with 100 mL of CH_2Cl_2, and the extract was washed with distilled water several times. The CH_2Cl_2 phase was dried with Na_2SO_4 and filtered, and the solvent was removed under vacuum. The material was redissolved in CH_2Cl_2, 100 mL of hydrochloric acid solution (~10% HCl) saturated with NaCl was added, and the CH_2Cl_2 solution was separated from the mixture, washed several times with water, dried with Na_2SO_4, and then chromatographed on alumina (80−200 mesh). Elution with CH_2Cl_2 removed a small amount of free base; [Mn(OEP)Cl] was eluted with a mixture of CH_2Cl_2 and methanol (3/1 v/v). Single crystals were obtained by recrystallization from acetone and hexanes. An X-ray analysis confirmed that the compound was [Mn(OEP)Cl].[14] IR (ν_{Mn-Cl}): 283 (m) cm^{-1}. UV/vis/near-IR: λ_{max} (ϵ, $cm^{-1}\ M^{-1}$) 358 (8.4×10^4), 424 (1.4×10^4), 471 (5.8×10^4), 558 (1.1×10^4), 589 (4.8×10^3), 685 (8.7×10^2), 780 (1.6×10^3) nm.

$[Mn(OEP)(H_2O)]ClO_4$ and $[Mn(OEP)(OClO_3)]$. A CH_2Cl_2 solution of [Mn(OEP)Cl] (0.4 g, 25 mL) was treated with an excess of aqueous $HClO_4$ (~4%, 200 mL). The CH_2Cl_2 phase was separated from the mixture and taken to dryness under vacuum. Recrystallization from CH_2Cl_2 and hexanes gave black platelike crystals of $[Mn(OEP)(H_2O)]ClO_4\cdot H_2O$. Very importantly, when drier conditions were used in the recrystallization (the CH_2Cl_2 phase was first dried with sufficient Na_2SO_4 and then taken to dryness under vacuum, and *freshly* distilled CH_2Cl_2 and hexanes were used as crystallization reagents), another species was isolated, which was identified as $[Mn(OEP)(OClO_3)]$ by X-ray crystallography.[15] The electronic spectra of $[Mn(OEP)(OClO_3)]$ and $[Mn(OEP)(H_2O)]ClO_4\cdot H_2O$ were identical; thus X-ray crystallography became the only convenient method to distinguish these two species. UV/vis/near-IR: λ_{max} (ϵ, $cm^{-1}\ M^{-1}$) 372 (8.5×10^4), 434 (1.7×10^4), 475 (2.0×10^4), 551 (9.4×10^3), 577 (sh, 6.1×10^3), 826 (1.7×10^3) nm. *Caution!* Although we have experienced no problem with the procedures described in dealing with systems containing perchlorate ion, they can detonate spontaneously and should be handled only in small quantities; in no case should such a system be heated above 30 °C and other safety precautions are also warranted.[16]

$\{[Mn(OEP)]_2(OH)\}ClO_4$. Method 1. Literature methods, or slight modifications thereof, for the synthesis of $[Fe(OEP)]_2O$[17] or $[Mn(TPP)]_2O$[18] were applied to the synthesis of $[Mn(OEP)]_2O$. We were unable to obtain single-crystal materials, but the isolated powders were employed in the synthesis of $\{[Mn(OEP)]_2(OH)\}ClO_4$. The above syntheses led to products with identical electronic spectra ($\lambda_{max}(CH_2Cl_2)$ 354 (Soret), 411, 462, 554, 582 (sh) nm) which are distinct from all the other known compounds, including [Mn(OEP)Cl], $[Mn(OEP)(H_2O)]ClO_4$, $[Mn(OEP)(OClO_3)]$, and $\{[Mn(OEP)]_2(OH)\}ClO_4$, thus suggesting a new species. This product is not stable in chlorocarbon solvents, and nearly complete conversion to [Mn(OEP)Cl] was detected by UV/vis spectra after 2 days. Identical spectra are also obtained in toluene.

A CH_2Cl_2 solution (15 mL) of $[Mn(OEP)]_2O$ (50 mg) was reacted with ~1 equiv of dilute aqueous $HClO_4$ (3.5 mL, 1.2×10^{-2} M). The CH_2Cl_2 phase was taken to dryness and recrystallized from CH_2Cl_2 and hexanes. A single crystal isolated from the first reaction confirmed the formulation of these crystals as $\{[Mn(OEP)]_2(OH)\}ClO_4\cdot 3CH_2Cl_2$; this crystalline compound gave the UV/vis spectrum described below. Unfortunately, a number of subsequent attempts to duplicate this procedure failed.

Method 2. A CH_2Cl_2 solution (75 mL) of [Mn(OEP)Cl] (1 g) was vigorously shaken with 100 mL of aqueous $HClO_4$ (~3% v/v) in a separatory funnel. The UV/vis spectrum indicated conversion of the starting material to $[Mn(OEP)(H_2O)]ClO_4$ or $[Mn(OEP)(OClO_3)]$. The CH_2Cl_2 layer was isolated and washed with distilled water several times. A UV/vis spectrum was taken after each washing. Water washes were continued until the blue shift of the Soret band from 372 to 350 nm was *just* complete. (Further washes led to the appearance of a new shoulder at ~354 nm.) The CH_2Cl_2 phase was isolated, dried with Na_2SO_4, and taken to dryness. Single crystals were obtained by recrystallization from CH_2Cl_2 and hexanes (4 days). $[Mn(OEP)(H_2O)]ClO_4$ and/or [Mn(OEP)Cl] are found as minor components if the above washing conditions are not carefully followed. UV/vis/near-IR (CH_2Cl_2): λ_{max} (ϵ, $cm^{-1}\ M^{-1}$) 349.5 (1.2×10^5), 459 (5.5×10^4), 560 (1.1×10^4), 593 (sh), 687 (1.3×10^3), 783 (2.1×10^3) nm.

(11) Naruta, Y.; Sasayama, M.-A.; Sasaki, T. *Angew. Chem., Int. Ed. Engl.* **1994**, *33*, 1839.
(12) Scheidt, W. R.; Cheng, B.; Safo, M. K.; Cukiernik, F.; Marchon, J.-C.; Debrunner, P. G. *J. Am. Chem. Soc.* **1992**, *114*, 4420.
(13) Adler, A. D.; Longo, F. R.; Kampas, F.; Kim, J. *J. Inorg. Nucl. Chem.* **1970**, *32*, 2443.
(14) Cheng, B.; Scheidt, W. R. Work in progress.
(15) Cheng, B.; Scheidt, W. R. *Acta Crystallogr., Sect. C* **1995**, *C51*, 825.
(16) Wolsey, W. C. *J. Chem. Educ.* **1973**, *50*, A335. *Chem. Eng. News* **1983**, *61* (Dec 5), 4; **1963**, *41* (July 8), 47.
(17) Cohen, I. A. *J. Am. Chem. Soc.* **1969**, *91*, 1980. La Mar, G. N.; Eaton, G. R.; Holm, R. H.; Walker, F. A. *J. Am. Chem. Soc.* **1973**, *95*, 63.
(18) Fleischer, E. B.; Palmer, J. M.; Srivastava, T. S.; Chatterjee, A. *J. Am. Chem. Soc.* **1971**, *93*, 3162.

Table 1. Crystal Data for $[Mn(OEP)(H_2O)]ClO_4 \cdot 2H_2O$ and $\{[Mn(OEP)]_2OH\}ClO_4 \cdot 3CH_2Cl_2$

	$[Mn(OEP)(H_2O)]ClO_4 \cdot H_2O$	$\{[Mn(OEP)]_2OH\}ClO_4 \cdot 3CH_2Cl_2$
formula	$C_{36}H_{48}ClMnN_4O_6$	$C_{75}H_{95}Cl_7Mn_2N_8O_5$
fw	723.17	1546.62
a, Å	12.800(1)	14.791(4)
b, Å	13.506(4)	14.895(2)
c, Å	13.355(7)	18.634(4)
α, deg	64.80(2)	69.79(2)
β, deg	62.36(3)	89.24(2)
γ, deg	85.67(3)	88.86(2)
V, Å^3	1829.1(11)	3851.7(14)
Z	2	2
space group	$P\bar{1}$	$P\bar{1}$
D_x, g/cm^3	1.313	1.334
$F(000)$	764	1620
μ, mm^{-1}	0.483	0.625
cryst dimens, mm	0.25 × 0.35 × 0.35	0.10 × 0.35 × 0.55
abs corr	DIFFABS	DIFFABS
λ, Å	0.710 73	0.710 73
T, °C	20(2)	−146(2)
no. of total data collected	17 316	37 254
no. of unique data	8891 (R_{int} = 0.0668)	19 422 (R_{int} = 0.0523)
no. of unique obsd data [$I > 2\sigma(I)$]	5715	15643
refinement method	on F^2 (SHELXL-93)	on F^2 (SHELXL-93)
final R indices for $I > 2\sigma(I)$	R_1 = 0.0754; wR_2 = 0.1897	R_1 = 0.0655; wR_2 = 0.1519
final R indices for all data	R_1 = 0.1220; wR_2 = 0.2210	R_1 = 0.0852; wR_2 = 0.1631

The desired complex could also be obtained from $[Mn(OEP)(H_2O)]ClO_4$ or $[Mn(OEP)(OClO_3)]$. In a typical preparation, a CH_2Cl_2 solution (150 mg, 20 mL) was washed with six 100-mL portions of distilled water. The reaction was followed by UV/vis spectroscopy, and the same product as above was confirmed. Recrystallization of the product as described above gave single crystals with unit cell parameters identical to those of $\{[Mn(OEP)]_2(OH)\}ClO_4 \cdot 3CH_2Cl_2$.

Sample Preparation for Magnetic Susceptibility Measurements. Sample 1. To 50 mL of a saturated CH_2Cl_2 solution of $\{[Mn(OEP)]_2(OH)\}ClO_4$ was added 150 mL of hexanes. The mixture was placed in a freezer (−20 °C) for fast crystallization. After 3 h, the mixture was filtered and the microcrystalline material of $\{[Mn(OEP)]_2(OH)\}ClO_4$ was obtained and dried under vacuum for 3 h. This sample was employed to measure the solid-state magnetic susceptibilities.

Sample 2. A large quantity of single-crystal $\{[Mn(OEP)]_2(OH)\}ClO_4 \cdot 3CH_2Cl_2$ was prepared as described above. Crystals, carefully selected according to their external shape, were crushed to powder and dried under vacuum for 3 h to remove all solvated CH_2Cl_2. The resulting powder sample was used to measure the magnetic susceptibilities in both the solid state and solution.

X-ray Structure Determinations. Black platelike crystals of $\{[Mn(OEP)]_2(OH)\}ClO_4 \cdot 3CH_2Cl_2$ (0.10 × 0.35 × 0.55 mm) and $[Mn(OEP)(H_2O)]ClO_4 \cdot H_2O$ (0.25 × 0.35 × 0.35 mm) were employed for X-ray structure determination on an Enraf-Nonius FAST area-detector diffractometer with a Mo rotating anode source ($\bar{\lambda}$ = 0.710 73 Å). Our detailed methods and procedures for small-molecule X-ray data collection with the FAST system have been described previously.[19] All measurements for $\{[Mn(OEP)]_2(OH)\}ClO_4 \cdot 3CH_2Cl_2$ were made at 127(1) K. However, the $[Mn(OEP)(H_2O)]ClO_4 \cdot H_2O$ crystal was extremely unstable under low temperature; thus room-temperature (T = 293(2) K) data were collected. A brief summary of crystal data and data collection parameters for the two structures is given in Table 1. Crystal decay was excluded by comparison of a common portion of data collected after each sweep during data collection. Data were corrected for Lorentz and polarization factors and, at the final stages of analysis, a modified version[20] of the absorption correction program DIFABS was applied.

Both structures were solved in the centrosymmetric space group $P\bar{1}$ using the direct methods program MULTAN;[22] difference Fourier syntheses for the two structures led to the location of all the remaining non-hydrogen atoms. Both structures were refined against F^2 with the program SHELXL-93.[23] All data collected were used, including negative intensities. All porphyrin hydrogen atoms in the two structures were idealized with the standard SHELXL-93 idealization methods. The hydroxo hydrogen atom in $\{[Mn(OEP)]_2(OH)\}ClO_4 \cdot 3CH_2Cl_2$ was directly located from a difference Fourier map and refined as an isotropic contributor. Severe disorder was observed for the perchlorate and two CH_2Cl_2 solvates in $\{[Mn(OEP)]_2(OH)\}ClO_4 \cdot 3CH_2Cl_2$. A well-resolved "rocking" disorder was found for the perchlorate anion in which the chlorine and two oxygen atoms each occupy two distinct positions, forming two conformers (Cl(1a), O(2), O(3), O(4a), O(5a) and Cl(1b), O(2), O(3), O(4b), O(5b)). The occupancies for the two conformers were initially taken from least-square refinement and then fixed at 0.6 and 0.4, respectively. For the first disordered CH_2Cl_2 molecule, the methylene carbon and one chlorine atom had two positions (C(2a) and C(2b); Cl(5a) and Cl(5b)) with occupancies of 0.6 and 0.4 and of 0.5 and 0.5, respectively; however, the other chlorine atom (Cl(4)) was fully occupied. The worst disordered region in the structure could be best explained with a model of three partially occupied CH_2Cl_2 molecules: Cl(6)−C(3)−Cl(7), Cl(8)−C(4)−Cl(9), and Cl(10)−C(5)−Cl(11), with occupancies of 0.28, 0.50, and 0.22, respectively. Atomic occupancies for the two disordered CH_2Cl_2 molecules were adjusted on the basis of their isotropic thermal parameters. The C−Cl bond lengths were constrained (with "DFIX 1.77" in SHELXL-93) for both disordered CH_2Cl_2 molecules in least-squares refinement. The solvated water molecule in $[Mn(OEP)(H_2O)]ClO_4 \cdot H_2O$ was also found to be disordered in three positions (O(6), O(7), and O(8)) with occupancies of 0.4, 0.4, and 0.2, respectively.

At convergence, the discrepancy indices[24] for $\{[Mn(OEP)]_2(OH)\}ClO_4 \cdot 3CH_2Cl_2$ ($[Mn(OEP)(H_2O)]ClO_4 \cdot H_2O$) are R_1 = 0.0655 (0.0754) for 15 643 (5715) observed data based on $F_o \geq 4.0\sigma(F_o)$, wR_2 = 0.1631 (0.2210) for 19 422 (8891) total unique data. Tables 2 and 3 give the atomic coordinates for $\{[Mn(OEP)]_2(OH)\}ClO_4$ and $[Mn(OEP)(H_2O)]$-

(19) Scheidt, W. R.; Turowska-Tyrk, I. *Inorg. Chem.* **1994**, *33*, 1314.
(20) The process is based on an adaptation of the DIFABS[21] logic to area detector geometry by: Karaulov, A. I. Personal Communication, School of Chemistry and Applied Chemistry, University of Wales, College of Cardiff, Cardiff CF1 3TB, U.K.
(21) Walker, N. P.; Stuart, D. *Acta Crystallogr., Sect. A* **1983**, *A39*, 158.
(22) A locally modified version of MULTAN78 was used: Main, P.; Hull, S. E.; Lessinger, L.; Germain, G.; Declercq, J. P.; Woolfson, M. M. MULTAN78: A System of Computer Programs for the Automatic Solution of Crystal Structures from X-ray Diffraction Data. Universities of York, England, and Louvain, Belgium, 1978.
(23) Sheldrick, G. M. *J. Appl. Crystallogr.*, in preparation.
(24) $R_1 = \sum||F_o| - |F_c||/\sum|F_o|$ and w$R_2 = \{\sum[w(F_o^2 - F_c^2)^2]/\sum[wF_o^4]\}^{1/2}$. The conventional R factors R_1 are based on F, with F set to zero for negative F^2. The criterion of $F^2 > 2\sigma(F^2)$ was used only for calculating R_1. R factors based on F^2 (wR_2) are statistically about twice as large as those based on F, and R factors based on ALL data will be even larger.

Table 2. Atomic Coordinates and Equivalent Isotropic Displacement Parameters (Å^2) for {[Mn(OEP)]$_2$OH}ClO$_4$·3CH$_2$Cl$_2$[a]

atom	*x*	*y*	*z*	*U*(eq)	atom	*x*	*y*	*z*	*U*(eq)
Mn(1)	0.48726(3)	0.67803(3)	0.65784(2)	0.0103(1)	2C(b2)	0.1469(2)	0.6222(2)	0.83318(15)	0.0151(5)
1N(1)	0.35341(14)	0.6970(2)	0.64548(12)	0.0125(4)	2C(b3)	0.3446(2)	0.3360(2)	0.86447(15)	0.0168(5)
1N(2)	0.47676(15)	0.5500(2)	0.64533(12)	0.0140(4)	2C(b4)	0.4289(2)	0.3095(2)	0.89200(15)	0.0158(5)
1N(3)	0.62227(15)	0.6692(2)	0.64639(12)	0.0136(4)	2C(b5)	0.6931(2)	0.4810(2)	0.94328(14)	0.0164(5)
1N(4)	0.49900(15)	0.81701(15)	0.64315(12)	0.0132(4)	2C(b6)	0.7081(2)	0.5729(2)	0.93849(15)	0.0169(5)
1C(a1)	0.3035(2)	0.7725(2)	0.65251(14)	0.0145(5)	2C(b7)	0.5143(2)	0.8650(2)	0.89362(15)	0.0161(5)
1C(a2)	0.2917(2)	0.6343(2)	0.63523(14)	0.0144(5)	2C(b8)	0.4246(2)	0.8862(2)	0.88083(15)	0.0161(5)
1C(a3)	0.3988(2)	0.5052(2)	0.63786(14)	0.0137(5)	2C(m1)	0.2929(2)	0.7944(2)	0.8629(2)	0.0154(5)
1C(a4)	0.5459(2)	0.4846(2)	0.65108(14)	0.0156(5)	2C(m2)	0.2507(2)	0.4845(2)	0.84121(15)	0.0150(5)
1C(a5)	0.6720(2)	0.5865(2)	0.65637(14)	0.0151(5)	2C(m3)	0.5561(2)	0.3948(2)	0.92579(14)	0.0155(5)
1C(a6)	0.6844(2)	0.7393(2)	0.63834(15)	0.0168(5)	2C(m4)	0.6089(2)	0.7176(2)	0.91446(15)	0.0155(5)
1C(a7)	0.5773(2)	0.8686(2)	0.63509(14)	0.0148(5)	2C(11)	0.0868(2)	0.7799(2)	0.8450(2)	0.0197(5)
1C(a8)	0.4310(2)	0.8756(2)	0.65344(14)	0.0149(5)	2C(21)	0.0612(2)	0.5796(2)	0.8187(2)	0.0200(5)
1C(b1)	0.2088(2)	0.7584(2)	0.64478(15)	0.01562(5)	2C(31)	0.2763(2)	0.2775(2)	0.8421(2)	0.0225(6)
1C(b2)	0.2020(2)	0.6740(2)	0.63242(15)	0.0164(5)	2C(41)	0.4776(2)	0.2161(2)	0.9045(2)	0.0197(5)
1C(b3)	0.4195(2)	0.4106(2)	0.63657(14)	0.0152(5)	2C(51)	0.7604(2)	0.4019(2)	0.9516(2)	0.0205(5)
1C(b4)	0.5109(2)	0.3984(2)	0.64419(14)	0.0153(5)	2C(61)	0.7961(2)	0.6201(2)	0.9401(2)	0.0249(6)
1C(b5)	0.7674(2)	0.6051(2)	0.6557(2)	0.0183(5)	2C(71)	0.5876(2)	0.9293(2)	0.9004(2)	0.0206(5)
1C(b6)	0.7750(2)	0.7003(2)	0.6424(2)	0.0195(5)	2C(81)	0.3749(2)	0.9768(2)	0.8747(2)	0.0247(6)
1C(b7)	0.5567(2)	0.9631(2)	0.63655(15)	0.0167(5)	2C(12)	0.0581(2)	0.7683(3)	0.9267(2)	0.0368(8)
1C(b8)	0.4664(2)	0.9666(2)	0.64958(15)	0.0168(5)	2C(22)	0.0213(2)	0.5071(2)	0.8908(2)	0.0287(7)
1C(m1)	0.3402(2)	0.8535(2)	0.66051(15)	0.0155(5)	2C(32)	0.2076(2)	0.2309(2)	0.9049(2)	0.0281(6)
1C(m2)	0.3128(2)	0.5449(2)	0.63228(14)	0.0153(5)	2C(42)	0.5338(3)	0.2181(2)	0.8345(2)	0.0317(7)
1C(m3)	0.6359(2)	0.5005(2)	0.65987(15)	0.0157(5)	2C(52)	0.7880(2)	0.3951(3)	0.8742(2)	0.0293(7)
1C(m4)	0.6631(2)	0.8330(2)	0.6313(2)	0.0183(5)	2C(62)	0.8287(2)	0.6794(3)	0.8604(2)	0.0381(8)
1C(11)	0.1354(2)	0.8277(2)	0.6469(2)	0.0219(6)	2C(72)	0.6366(2)	0.9768(3)	0.8249(2)	0.0332(7)
1C(21)	0.1187(2)	0.6298(2)	0.6144(2)	0.0228(6)	2C(82)	0.3255(3)	0.9694(3)	0.9488(2)	0.0383(8)
1C(31)	0.3519(2)	0.3436(2)	0.6254(2)	0.0206(5)	O(1)	0.49039(14)	0.63452(14)	0.77194(10)	0.0155(4)
1C(41)	0.5679(2)	0.3163(2)	0.6398(2)	0.0200(5)	H	0.5393(33)	0.6291(34)	0.7809(27)	0.048(14)
1C(51)	0.8418(2)	0.5326(2)	0.6645(2)	0.0230(6)	Cl(1a)[b]	0.1593(3)	1.0763(2)	0.72941(14)	0.0275(5)
1C(61)	0.8596(2)	0.7576(2)	0.6310(2)	0.0302(7)	Cl(1b)[c]	0.1524(4)	1.0592(3)	0.7569(2)	0.0336(10)
1C(71)	0.6247(2)	1.0407(2)	0.6227(2)	0.0195(5)	O(2)	0.2203(2)	1.1398(2)	0.7392(2)	0.0555(9)
1C(81)	0.4101(2)	1.0484(2)	0.6555(2)	0.0226(6)	O(3)	0.1980(2)	0.9887(2)	0.7313(2)	0.0485(7)
1C(12)	0.1232(2)	0.9097(3)	0.5713(2)	0.0350(8)	O(4a)[b]	0.1141(4)	1.1158(4)	0.6587(3)	0.0569(14)
1C(22)	0.1099(3)	0.6481(3)	0.5290(2)	0.0397(9)	O(5a)[b]	0.0933(5)	1.0586(5)	0.7899(4)	0.067(2)
1C(32)	0.3294(2)	0.3664(2)	0.5415(2)	0.0285(7)	O(4b)[c]	0.0660(5)	1.0933(6)	0.7271(6)	0.057(2)
1C(42)	0.6099(3)	0.3365(2)	0.5603(2)	0.0336(8)	O(5b)[c]	0.1458(6)	1.0088(6)	0.8380(5)	0.059(2)
1C(52)	0.8678(3)	0.5183(3)	0.5899(2)	0.0415(9)	C(1)	0.0563(3)	1.3010(3)	0.7084(3)	0.0464(10)
1C(62)	0.8812(3)	0.8094(3)	0.5473(3)	0.0510(11)	Cl(2)	0.02896(7)	1.37285(7)	0.76322(6)	0.0454(2)
1C(72)	0.6485(3)	1.0874(2)	0.5381(2)	0.0301(7)	Cl(3)	0.09398(7)	1.37001(8)	0.61635(7)	0.0481(2)
1C(82)	0.3654(3)	1.1067(2)	0.5803(2)	0.0384(8)	C(2a)[b]	−0.0687(12)	1.0467(9)	0.8743(10)	0.121(6)
Mn(2)	0.43072(2)	0.60140(3)	0.87607(2)	0.0100(1)	C(2b)[c]	−0.0616(19)	1.0393(13)	0.9430(18)	0.157(12)
2N(1)	0.29871(14)	0.6325(2)	0.85746(12)	0.0124(4)	Cl(4)	−0.1317(2)	0.9602(2)	0.9343(2)	0.1685(15)
2N(2)	0.40659(15)	0.4658(2)	0.88585(12)	0.0131(4)	Cl(5a)[d]	−0.1327(8)	1.1485(6)	0.8770(5)	0.204(4)
2N(3)	0.55518(14)	0.5612(2)	0.91932(12)	0.0130(4)	Cl(5b)[d]	−0.0613(3)	1.1515(3)	0.8932(2)	0.087(2)
2N(4)	0.44681(14)	0.7291(2)	0.88741(12)	0.0126(4)	C(3)[e]	−0.0968(14)	1.0821(14)	0.6966(15)	0.080(7)
2C(a1)	0.2529(2)	0.7148(2)	0.85569(14)	0.0144(5)	Cl(6)[e]	−0.1785(9)	1.1712(9)	0.6764(8)	0.078(3)
2C(a2)	0.2342(2)	0.5756(2)	0.84302(14)	0.0137(5)	Cl(7)[e]	−0.1197(5)	0.9902(7)	0.6653(8)	0.089(3)
2C(a3)	0.3306(2)	0.4330(2)	0.86191(15)	0.0146(5)	C(4)[d]	−0.1026(11)	1.0634(16)	0.6519(9)	0.150(13)
2C(a4)	0.4682(2)	0.3911(2)	0.90373(14)	0.0148(5)	Cl(8)[d]	−0.1268(3)	0.9481(4)	0.7254(3)	0.0809(11)
2C(a5)	0.5979(2)	0.4747(2)	0.93088(14)	0.0145(5)	Cl(9)[d]	−0.1651(5)	1.1538(5)	0.6658(4)	0.116(3)
2C(a6)	0.6223(2)	0.6223(2)	0.92371(14)	0.0140(5)	C(5)[f]	−0.0536(13)	0.9861(32)	0.7035(11)	0.126(18)
2C(a7)	0.5275(2)	0.7673(2)	0.89846(14)	0.0140(5)	Cl(10)[f]	−0.1267(6)	0.9251(6)	0.7764(7)	0.091(3)
2C(a8)	0.3833(2)	0.8018(2)	0.87593(14)	0.0145(5)	Cl(11)[f]	−0.1136(7)	1.0262(8)	0.6195(5)	0.081(3)
2C(b1)	0.1578(2)	0.7076(2)	0.84308(15)	0.0149(5)					

[a] The estimated standard deviations of the least significant digits are given in parentheses. *U*(eq) is defined as one-third of the trace of the orthogonalized $\mathbf{U}_{ij}$ tensor. [b] Occupancy number of 0.6. [c] Occupancy number of 0.4. [d] Occupancy number of 0.5. [e] Occupancy number of 0.28. [f] Occupancy number of 0.22.

ClO_4, respectively. The complete crystallographic details, anisotropic thermal parameters, and the fixed hydrogen atom coordinates for the two structures are included in the supporting information (Tables S1−S3 for {[Mn(OEP)]$_2$(OH)}ClO$_4$·3CH$_2$Cl$_2$ and Tables S4−S6 for [Mn(OEP)(H$_2$O)]ClO$_4$·H$_2$O).

Magnetic Susceptibility Measurements. The Evans NMR method was used to obtain solution magnetic susceptibilities.[25] A $CDCl_3$ solution of sample 1 of {[Mn(OEP)]$_2$(OH)}ClO$_4$ (0.2 mL, $C = 9.0 \times 10^{-3}$ M) was tranferred to the inner tube, and 0.25 mL of $CDCl_3$, to the outer tube. NMR spectra were then recorded at 20 °C, and the line shift of $CHCl_3$ was measured to calculate the solution susceptibility.

Solid-state magnetic susceptibilities were measured under helium on a Quantum Design MPMS SQUID susceptometer from 2 to 305 K at a field of 0.5 T. The samples (15−20 mg) were contained in a Kel-F bucket. The bucket had been calibrated independently at the same field and temperatures. Each raw data file was corrected for the diamagnetic contribution of both the sample holder and the compound to the susceptibility, using Pascal's constants for the metal, axial ligand, and counteranion and a measured value $\chi_M = -481 \times 10^{-6}$ cgs emu for H$_2$(OEP).

As detailed in the Appendix, the magnetic susceptibilities $\chi_{\parallel}$, $\chi_{\perp}$, and $\chi = (\chi_{\parallel} + 2\chi_{\perp})/3$ were derived for the pure dimer {[Mn(OEP)]$_2$(OH)}ClO$_4$ in the actual geometry (Mn(1)−O−Mn(2) bridge angle = 152.73°) found by X-ray crystallography. Each Mn(III) center of the dimer was treated as an axially anisotropic, zero-field-split, high-spin

(25) Evans, D. F. *J. Chem. Soc.* **1959**, 2003. Bartle, K. D.; Dale, B. J.; Jones, D. W.; Maricic, S. *J. Magn. Reson.* **1973**, *12*, 286.

Table 3. Atomic Coordinates and Equivalent Isotropic Displacement Parameters (Å^2) for $[Mn(OEP)(H_2O)]ClO_4 \cdot H_2O$[a]

atom	*x*	*y*	*z*	*U*(eq)
Mn	0.63859(5)	0.46056(4)	0.81053(5)	0.0387(2)
N(1)	0.5238(3)	0.5686(2)	0.8059(3)	0.0414(6)
N(2)	0.7729(3)	0.5842(2)	0.6733(3)	0.0430(7)
N(3)	0.7570(3)	0.3618(2)	0.8356(3)	0.0423(6)
N(4)	0.5067(3)	0.3445(2)	0.9657(3)	0.0414(6)
C(a1)	0.4017(3)	0.5473(3)	0.8866(3)	0.0426(8)
C(a2)	0.5466(3)	0.6753(3)	0.7150(4)	0.0465(8)
C(a3)	0.7636(3)	0.6871(3)	0.5965(3)	0.0461(8)
C(a4)	0.8945(3)	0.5801(3)	0.6260(3)	0.0441(8)
C(a5)	0.8794(3)	0.3877(3)	0.7701(4)	0.0451(8)
C(a6)	0.7321(3)	0.2499(3)	0.9163(4)	0.0462(8)
C(a7)	0.5136(3)	0.2350(3)	1.0288(3)	0.0444(8)
C(a8)	0.3876(3)	0.3533(3)	1.0241(3)	0.0441(8)
C(b1)	0.3484(3)	0.6435(3)	0.8449(4)	0.0478(8)
C(b2)	0.4379(4)	0.7223(3)	0.7394(4)	0.0538(9)
C(b3)	0.8819(4)	0.7480(3)	0.4988(3)	0.0506(9)
C(b4)	0.9619(4)	0.6826(3)	0.5191(3)	0.0502(9)
C(b5)	0.9319(4)	0.2917(4)	0.8137(4)	0.0517(9)
C(b6)	0.8419(4)	0.2069(3)	0.9000(4)	0.0504(9)
C(b7)	0.3955(4)	0.1754(3)	1.1270(3)	0.0482(9)
C(b8)	0.3179(3)	0.2485(3)	1.1249(3)	0.0475(8)
C(m1)	0.3402(3)	0.4492(3)	0.9886(4)	0.0476(8)
C(m2)	0.6590(4)	0.7286(3)	0.6151(4)	0.0524(9)
C(m3)	0.9427(3)	0.4890(3)	0.6743(4)	0.0498(9)
C(m4)	0.6188(4)	0.1909(3)	1.0036(4)	0.0486(9)
C(11)	0.2169(4)	0.6467(4)	0.9069(4)	0.0563(10)
C(21)	0.4297(5)	0.8394(4)	0.6623(6)	0.085(2)
C(31)	0.9047(5)	0.8633(4)	0.3967(4)	0.0645(12)
C(41)	1.0956(4)	0.7099(4)	0.4494(4)	0.0640(11)
C(51)	1.0634(4)	0.2945(4)	0.7714(5)	0.0636(11)
C(61)	0.8503(4)	0.0892(4)	0.9705(4)	0.0629(11)
C(71)	0.3681(4)	0.0535(4)	1.2123(4)	0.0658(12)
C(81)	0.1849(4)	0.2277(4)	1.2034(4)	0.0621(11)
C(12)	0.1520(5)	0.5981(5)	0.8644(6)	0.0791(14)
C(22)	0.3782(10)	0.8533(6)	0.5819(9)	0.179(5)
C(32)	0.9030(7)	0.9525(4)	0.4349(6)	0.102(2)
C(42)	1.1445(5)	0.7456(6)	0.5140(6)	0.094(2)
C(52)	1.1022(5)	0.3479(6)	0.8308(6)	0.092(2)
C(62)	0.8639(6)	0.0657(5)	1.0852(5)	0.092(2)
C(72)	0.3378(6)	−0.0132(5)	1.1610(6)	0.100(2)
C(82)	0.1224(5)	0.2198(5)	1.1356(5)	0.083(2)
O(1)	0.6243(3)	0.4125(3)	0.6827(3)	0.0647(8)
Cl	0.4111(2)	0.1959(2)	0.7376(2)	0.1201(7)
O(2)	0.4081(9)	0.0873(6)	0.7767(13)	0.312(7)
O(3)	0.3489(7)	0.2305(7)	0.6701(7)	0.183(3)
O(4)	0.3607(14)	0.2321(16)	0.8223(13)	0.402(12)
O(5)	0.5299(7)	0.2366(8)	0.6683(12)	0.252(5)
O(6)[b]	0.6679(16)	0.5250(16)	0.4519(13)	0.155(7)
O(7)[b]	0.5694(26)	0.5624(10)	0.5134(20)	0.159(9)
O(8)[c]	0.4286(47)	0.5584(24)	0.6066(31)	0.166(16)

[a] The estimated standard deviations of the least significant digits are given in parentheses. *U*(eq) is defined as one-third of the trace of the orthogonalized $\mathbf{U}_{ij}$ tensor. [b] Occupancy number of 0.4. [c] Occupancy number of 0.2.

d^4 system with a *g* value set at 2.0. The monomeric impurity present in the dimer samples was assumed to be $[Mn(OEP)(H_2O)]ClO_4$, which was treated either as an isotropic ($g = 2.0$, $D = 0$) $S = 2$ system or as a zero-field-split ($g = 2.0$, $D = -2.3$ cm^{-1}) $S = 2$ system.[26] Calculated values were obtained through a least-squares fit of eq 1, which relates

$$\chi = M_{di}[(1 - w_{mo})\chi_{di} + w_{mo}\chi_{mo}]/[(1 - w_{mo})M_{di} + w_{mo}M_{mo}] \quad (1)$$

the sample susceptibility to the susceptibilities of the dimer and monomer. In this expression, w_{mo} is the mole fraction of the monomer, M_{di} and M_{mo} are the molecular weights of the dimer and monomer, and χ_{di} and χ_{mo} are their respective powder susceptibilities (see Appendix). The fitting procedure was carried out with "an2g.f", a locally written FORTRAN program (**an**isotropic Hamiltonian of **2** **g**eneral spins) about 3000 statements long.

(26) Kennedy, B. J.; Murray, K. S. *Inorg. Chem.* **1985**, *24*, 1557.

Similar spin Hamiltonian techniques have been employed by Day et al.[27] for describing the magnetic properties of binuclear sites. However, their formalism was restricted to particular orientations of the zero-field-splitting (ZFS) tensors of both sites. Our method is general. Based on the techniques of the Wigner rotation matrix as explained in the Appendix, it applies to the actual orientation of the ZFS tensors of the magnetic centers.

Results

X-ray Structure of $[Mn(OEP)(H_2O)]ClO_4 \cdot H_2O$. Figure 1 displays the structure and the labeling scheme for the $[Mn(OEP)(H_2O)]^+$ ion. Selected bond distances and angles are given in Table 4, and the full listings are provided as supporting information. Averaged values for the chemical classes of distances and angles in the porphinato core are entered on the mean plane diagram given in Figure 2, which also shows the perpendicular displacements of each atom (in units of 0.01 Å) from the mean plane of the 24-atom core. The four $Mn-N_p$ bond distances have an average value of 1.996(4) Å, and the axial $Mn-O_{H_2O}$ bond length is 2.149(3) Å. The displacement of the manganese(III) atom from the mean porphinato core is 0.17 Å.

A pair of metalloporphyrin cations form a "face-to-face" $\pi-\pi$ dimer with a Ct···Ct distance of 4.924 Å, an inter-ring distance of 3.504 Å, and a lateral shift[28] of 3.459 Å. The four "up"/four "down" orientation of the ethyl groups is commonly seen for octaethylporphyrin derivatives with this degree of inter-ring overlap.[28] The two rings are precisely parallel as they are related by an inversion center. An ORTEP diagram showing these structural features is included in the supporting information. The dimers are well-separated in the lattice with no extended hydrogen-bonding network involving the perchlorate, solvate, and ligand water molecules, unlike that found in $[Fe(OEP)(H_2O)]ClO_4 \cdot 2H_2O$.[29]

X-ray Structure of $\{[Mn(OEP)]_2(OH)\}ClO_4$. Figures 3 and 4 are ORTEP diagrams of the $\{[Mn(OEP)]_2(OH)\}^+$ cation. Figure 4 also illustrates the labeling scheme used in the tables for the non-hydrogen atoms. For ring 2, since the labeling of the atoms is exactly the same as that in ring 1, only the four pyrrole nitrogen atoms are labeled. In all tables, the atom names of ring 1 are preceded by the numeral "1" and those of ring 2 by "2". Individual bond distances and bond angles are given in Tables 5 and 6, respectively. Averaged values for the unique chemical classes of distances and angles in the porphinato cores are entered on the mean plane diagram given in Figure 5, which also displays the perpendicular displacement of each atom (in units of 0.01 Å) from the mean plane of the 24-atom core.

As seen in Figure 4, a most striking feature of the $\{[Mn(OEP)]_2(OH)\}^+$ cation is that the two porphyrin units have a nearly eclipsed inter-ring orientation with an average N−Mn−Mn′−N′ dihedral angle of 4.3°. The two porphyrin rings are not parallel but rather form a dihedral angle of 12.7°. The plane defined by the two manganese ions and oxygen and hydrogen of the bridging hydroxide are seen to lie in one of the N−Mn−Mn′−N′ "planes", and since the two porphyrin rings are "hinged" at the bridging oxygen atom, the closest inter-ring atoms will be those of the two pyrrole rings directly opposite the bridging oxygen atom. The nearly overlapped $C_b \cdots C_b$ atoms are at distances of 3.58 and 3.63 Å; the distance between

(27) Day, E. P.; Kent, T. A.; Lindahl, P. A.; Münck, E.; Orme-Johnson, W. H.; Roder, H.; Roy, A. *Biophys. J.* **1987**, *52*, 837. Yu, S.-B.; Wang, C.-P.; Day, E. P.; Holm, R. H. *Inorg. Chem.* **1991**, *30*, 4067. Hendrich, M. P.; Day, E. P.; Wang, C.-P.; Synder, B. S.; Holm, R. H.; Münck, E. *Inorg. Chem.* **1994**, *33*, 2848.

(28) Scheidt, W. R.; Lee, Y. J. *Struct. Bonding* **1987**, *64*, 1.

(29) Cheng, B.; Safo, M. K.; Orosz, R. D.; Reed, C. A.; Debrunner, P. G.; Scheidt, W. R. *Inorg. Chem.* **1994**, *33*, 1319.

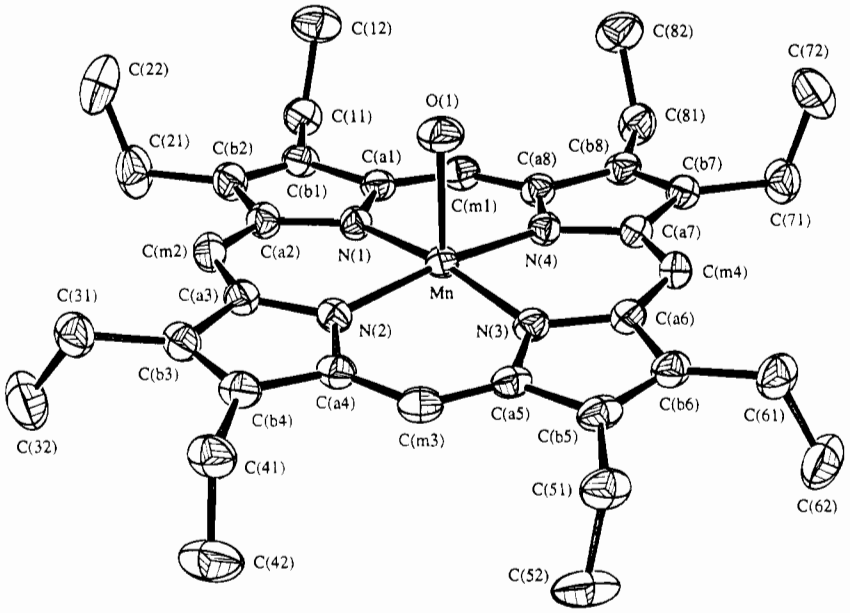

Figure 1. ORTEP diagram with atom-labeling scheme for $[Mn(OEP)(H_2O)]ClO_4$. Thermal ellipsoids are drawn at the 30% probability level. Porphyrin hydrogen atoms are omitted for clarity.

overlapped methylene carbon atoms are similar (3.58 and 3.71 Å). The two cores have approximately S_4-ruffled cores; the largest deviation from such idealized symmetry occurs in pyrrole rings 1, which are the close pair of pyrrole rings. Figure 3 shows the ethyl group orientations; all ethyl groups are oriented away from each other in the region between the closest approach of the two porphyrin rings.

The hydroxide hydrogen atom was found in a difference Fourier map, and its positional coordinates and temperature factor were successfully refined in least squares. The Mn_2OH entity is essentially planar. The two Mn−O−H angles are 104(4) and 103(4)°, and the Mn−O(H)−Mn angle is 152.73(11)°. The Mn(1)···Mn(2) separation is 3.909(1) Å. The hydroxide oxygen and hydrogen atoms are well-separated from any atoms other than the porphyrin atoms in the dinuclear complex. In particular, there is no hydrogen-bonding interaction between either the oxygen or hydrogen of the hydroxide ion. The closest perchlorate ion atom is >6.5 Å away. Indeed, the closest approach to the atoms of the hydroxide ion are intermolecular contacts to an α-carbon of an adjacent porphyrin ring (5.4 Å).

The average Mn−N_p bond distances in the two porphinato cores are identical at Mn(1)−N_p = 2.006(7) and Mn(2)−N_p = 2.007(5) Å. The two manganese ions are displaced by 0.19 and 0.23 Å from their respective 24-atom mean plane (Figure 5), each toward the bridging hydroxide group. Despite this, there are significant differences in the geometry of the two manganese(III) sites in $\{[Mn(OEP)]_2(OH)\}ClO_4$. The two Mn−O(OH) distances are slightly different at 1.998(2) and 2.024(2) Å. More significant are the differences along the axial Mn−O direction. In neither porphyrin is the Mn−O vector precisely perpendicular to the porphinato plane; the deviations are readily seen in the spread of N_p−Mn−O angles, which average to 96.4(2.3)° at Mn(1) and 95.9(8.4)° at Mn(2). The spread at Mn(2) is much larger with the smallest angle value = 86.15(9) and the largest = 106.55(9)°; the corresponding values at Mn(1) are much closer at 94.20(9) and 98.88(9)°.

Magnetism. The temperature dependence of χT for the mononuclear Mn(III) complex $[Mn(OEP)(H_2O)]ClO_4$ in the range 2−300 K is typical of that expected for an isotropic S = 2 system: χT remains constant (χT = 3.0) over the entire temperature range. Fitting of the data led to a value D = 0, *i.e.* a simple Cure law. We also tried an axially anisotropic model through inclusion of a zero-field-splitting term ($D = -2.3$ cm^{-1}); the latter is equal to that found earlier for the so-called perchlorate complex "$Mn(OEP)ClO_4 \cdot H_2O$",[26] which is presumably identical to the structurally characterized species $[Mn(OEP)(H_2O)]ClO_4$ investigated here. This model also led to a very good fit. The observed χT values are given in the supporting information (Table S8).

The temperature dependence of χ for samples 1 and 2 of the hydroxo-bridged dimer $\{[Mn(OEP)]_2(OH)\}ClO_4$ is shown in Figure 6. The observed behavior is typical of an exchanged-coupled dinuclear complex containing a residual mononuclear impurity. Crystallite orientation in the magnetic field at low temperatures, which is particularly prevalent in mononuclear high-spin Mn(III) porphyrins,[26] did not occur in the dinuclear complex, as indicated by the fact that nearly identical χ vs T curves were obtained for increasing or decreasing temperatures. The data were fit to the total spin Hamiltonian of a zero-field-split, high-spin d^4−d^4 dimer, including an S = 2 impurity. The computational methodology is detailed in the Appendix. Satisfactory fits were obtained with a value of $J = -35.2 \pm 0.2$ cm^{-1} and $D = +14 \pm 4$ cm^{-1}, with $w_{mo} = \sim 1-2\%$ for a Curie-like impurity. Since the adjusted parameter D appeared too large in absolute value and opposite in expected sign, additional calculations were carried out. It soon became evident that satisfactory fits could be obtained by constraining D to negative values and that, using this methodology, the sign of D could not be unambiguously determined nor its absolute value known accurately.[26,30] However, all calculations led consistently to J values close to -35 cm^{-1}, which leads us to consider that an antiferromagnetic coupling of this magnitude is the dominant physical phenomenon in the dimer, with zero-field splitting being only second-order. In view of the axially elongated structure around Mn(III) in the dimer, a negative sign is expected for D.[31] Furthermore, inclusion of a zero-field-splitting term ($D = -2.3$ cm^{-1}) for the mononuclear impurity led to lower, more reasonable, absolute value of D for the dimer. With these observations in mind, we offer the following set of parameters for the dimer as best final values of the fits: $J = -35.5 \pm 0.2$

(30) Behere, D. V.; Marathe, V. R.; Mitra, S. *Chem. Phys. Lett.* **1981**, *81*, 57.
(31) Bertoncello, K.; Fallon, G. D.; Murray, K. S.; Tiekink, E. R. T. *Inorg. Chem.* **1991**, *30*, 3562.

Table 4. Selected Bond Lengths (Å) and Angles (deg) for $[Mn(OEP)(H_2O)]ClO_4 \cdot H_2O$[a]

Mn−O(1)	2.149(3)	C(a5)−C(b5)	1.436(5)
Mn−N(1)	1.994(3)	C(a6)−C(b6)	1.435(5)
Mn−N(2)	2.002(3)	C(a7)−C(b7)	1.449(5)
Mn−N(3)	1.993(3)	C(a8)−C(b8)	1.437(5)
Mn−N(4)	1.997(3)	C(a1)−C(m1)	1.363(5)
N(1)−C(a1)	1.388(5)	C(a2)−C(m2)	1.388(6)
N(1)−C(a2)	1.371(4)	C(a3)−C(m2)	1.366(6)
N(2)−C(a3)	1.368(5)	C(a4)−C(m3)	1.374(5)
N(2)−C(a4)	1.389(5)	C(a5)−C(m3)	1.371(6)
N(3)−C(a5)	1.376(5)	C(a6)−C(m4)	1.383(5)
N(3)−C(a6)	1.383(5)	C(a7)−C(m4)	1.381(5)
N(4)−C(a7)	1.376(4)	C(a8)−C(m1)	1.376(5)
N(4)−C(a8)	1.377(5)	C(b1)−C(b2)	1.357(6)
C(a1)−C(b1)	1.438(5)	C(b3)−C(b4)	1.349(6)
C(a2)−C(b2)	1.438(5)	C(b5)−C(b6)	1.344(6)
C(a3)−C(b3)	1.454(5)	C(b7)−C(b8)	1.348(6)
C(a4)−C(b4)	1.433(5)		
N(1)−Mn−O(1)	95.31(12)	N(4)−C(a8)−C(b8)	111.3(3)
N(2)−Mn−O(1)	93.85(13)	C(m1)−C(a1)−N(1)	125.4(3)
N(3)−Mn−O(1)	95.20(12)	C(m2)−C(a2)−N(1)	124.2(3)
N(4)−Mn−O(1)	95.07(13)	C(m2)−C(a3)−N(2)	124.7(3)
N(1)−Mn−N(2)	89.35(12)	C(m3)−C(a4)−N(2)	124.2(3)
N(1)−Mn−N(3)	169.47(12)	C(m3)−C(a5)−N(3)	125.3(3)
N(1)−Mn−N(4)	89.76(12)	C(m4)−C(a6)−N(3)	124.8(3)
N(2)−Mn−N(3)	89.43(13)	C(m4)−C(a7)−N(4)	124.4(3)
N(2)−Mn−N(4)	171.08(12)	C(m1)−C(a8)−N(4)	124.6(3)
N(3)−Mn−N(4)	89.82(13)	C(m1)−C(a1)−C(b1)	124.6(4)
C(a1)−N(1)−Mn	126.8(2)	C(m2)−C(a2)−C(b2)	125.8(4)
C(a2)−N(1)−Mn	127.1(2)	C(m2)−C(a3)−C(b3)	125.4(4)
C(a3)−N(2)−Mn	126.5(3)	C(m3)−C(a4)−C(b4)	125.0(4)
C(a4)−N(2)−Mn	127.6(3)	C(m3)−C(a5)−C(b5)	124.7(4)
C(a5)−N(3)−Mn	127.6(3)	C(m4)−C(a6)−C(b6)	125.7(4)
C(a6)−N(3)−Mn	126.4(2)	C(m4)−C(a7)−C(b7)	125.9(3)
C(a7)−N(4)−Mn	126.9(3)	C(m1)−C(a8)−C(b8)	124.0(4)
C(a8)−N(4)−Mn	127.5(2)	C(b2)−C(b1)−C(a1)	106.7(3)
C(a1)−N(1)−C(a2)	105.8(3)	C(b1)−C(b2)−C(a2)	107.4(3)
C(a3)−N(2)−C(a4)	105.4(3)	C(b4)−C(b3)−C(a3)	107.5(3)
C(a5)−N(3)−C(a6)	105.9(3)	C(b3)−C(b4)−C(a4)	106.5(3)
C(a7)−N(4)−C(a8)	105.2(3)	C(b6)−C(b5)−C(a5)	107.0(3)
N(1)−C(a1)−C(b1)	110.0(3)	C(b5)−C(b6)−C(a6)	107.7(3)
N(1)−C(a2)−C(b2)	110.0(3)	C(b8)−C(b7)−C(a7)	107.7(3)
N(2)−C(a3)−C(b3)	109.8(3)	C(b7)−C(b8)−C(a8)	106.1(3)
N(2)−C(a4)−C(b4)	110.8(3)	C(a1)−C(m1)−C(a8)	125.6(4)
N(3)−C(a5)−C(b5)	109.9(3)	C(a2)−C(m2)−C(a3)	126.0(4)
N(3)−C(a6)−C(b6)	109.3(3)	C(a4)−C(m3)−C(a5)	125.6(4)
N(4)−C(a7)−C(b7)	109.7(3)	C(a6)−C(m4)−C(a7)	125.6(3)

[a] Estimated standard deviations of the least significant digits are given in parentheses.

cm^{-1}, $D = -8 \pm 2\ cm^{-1}$, $w_{mo} = \sim 1-2\%$. The solid lines shown in Figure 6 were calculated using this set of parameters.

A solution susceptibility was measured by NMR methods for $\{[Mn(OEP)]_2(OH)\}ClO_4$ in $CDCl_3$. The effective magnetic moment at 20 °C was 3.4 μ_B.

Discussion

Syntheses. Our initial strategy for the synthesis of the $\{[Mn(OEP)]_2(OH)\}ClO_4$ complex was to protonate the oxo bridge of $[Mn(OEP)]_2O$, i.e., to follow the synthetic procedure we used for the μ-hydroxo iron complex.[12] This procedure provided a single crystal[32] of the desired $\{[Mn(OEP)]_2(OH)\}ClO_4$ species, but the preparation was not uniformly reproducible, possibly because of the presence of basic impurities in the noncrystalline $[Mn(OEP)]_2O$ intermediate. This led us to attempt more straightforward syntheses of $\{[Mn(OEP)]_2(OH)\}ClO_4$ starting from monomeric manganese(III) derivatives, such as [Mn(OEP)Cl], $[Mn(OEP)(H_2O)]ClO_4$, or $[Mn(OEP)(OClO_3)]$.

(32) A single-crystal structure analysis was applied to one of the crystals obtained. The structural results are identical to those obtained for subsequent crystalline samples, which are reported herein.

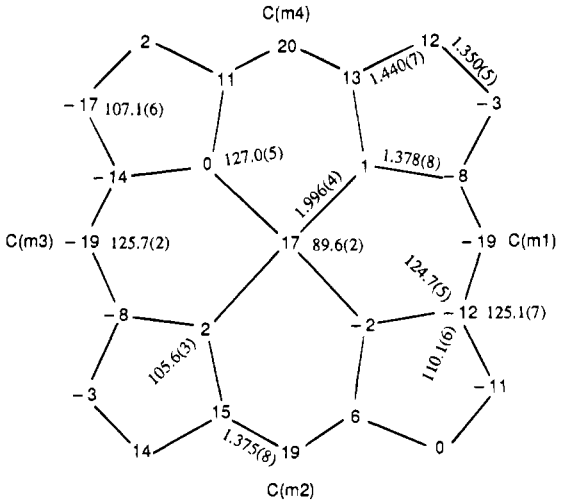

Figure 2. Formal diagram of the porphinato core of $[Mn(OEP)(H_2O)]ClO_4$, displaying the average values for the bond parameters. The numbers in parentheses are the estimated standard deviations calculated on the assumption that the averaged values were all drawn from the same population. Also displayed are the perpendicular displacements, in units of 0.01 Å, of each atom from the 24-atom mean plane of the core.

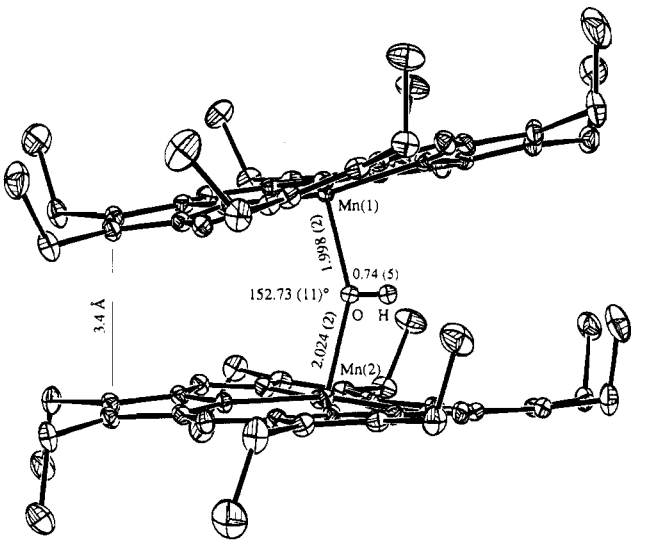

Figure 3. "Edge view" ORTEP diagram of $\{[Mn(OEP)]_2(OH)\}ClO_4$. Thermal ellipsoids are drawn at the 50% probability level. Porphyrin hydrogen atoms are omitted for clarity. The Mn−O(H)−Mn bridge is in the plane of the paper.

All of these, as described in the Experimental Section, lead to the *reproducible* synthesis of $\{[Mn(OEP)]_2(OH)\}ClO_4$.

We have followed the preparative reactions by UV/vis spectroscopy. The reaction can be easily monitored, and spectra of the starting complex, the final species, and an intermediate reaction stage are illustrated in Figure 7. We observe that no matter which monomeric compound is used, the starting complex is always converted to $[Mn(OEP)(H_2O)]^+$ and/or $[Mn(OEP)(OClO_3)]$ rather than forming a μ-oxo derivative. Thus the immediate precursor in the synthesis appears to be monomeric. Unfortunately, there is no convenient way to distinguish between $[Mn(OEP)(H_2O)]^+$ and $[Mn(OEP)(OClO_3)]$ since they show identical electronic spectra. However, in this biphasic CH_2Cl_2/H_2O reaction system, formation of $[Mn(OEP)(H_2O)]^+$ is much more likely than formation of $[Mn(OEP)(OClO_3)]$. We have been unable to completely define the stoichiometry of the reaction because of its biphasic nature, but it is nontheless clear that a hydrolysis reaction occurs. Although there is no spectral

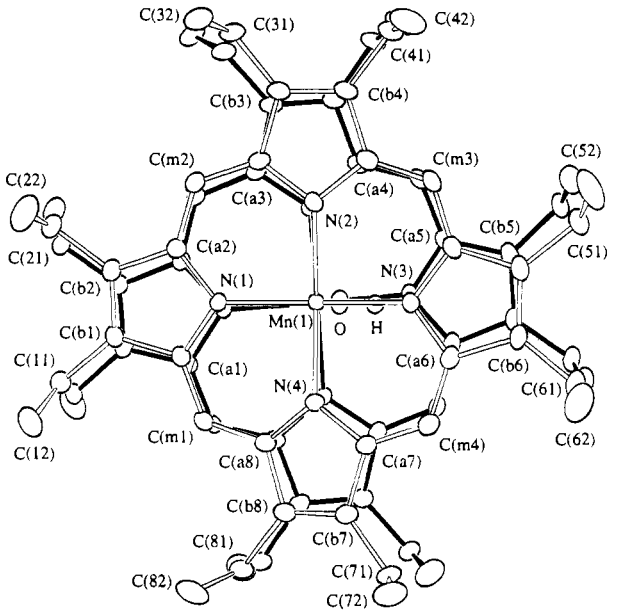

Figure 4. "Top view" ORTEP diagram of $\{[Mn(OEP)]_2(OH)\}ClO_4$ with atom-labeling scheme. The Mn(1)···Mn(2) axis is perpendicular to the plane of the paper. Thermal ellipsoids are drawn at the 50% probability level. Porphyrin ring 2 is drawn with solid bonds while ring 1 is drawn with open bonds. The atom-labeling scheme for ring 2 is identical to that of ring 1; equivalent atoms lie almost directly below those of ring 1.

evidence for a μ-oxo derivative during these preparative reactions, the reaction described in the previous paragraph does show that the oxo bridge can be protonated. Morever, UV/vis spectral data suggest that the μ-oxo derivative can be prepared by deprotonation of $\{[Mn(OEP)_2(OH)\}ClO_4$. The spectrum obtained when a CH_2Cl_2 solution of $\{[Mn(OEP)]_2(OH)\}ClO_4$ is made basic is shown in Figure 8. Interestingly, halocarbon solutions of $\{(Mn(OEP)]_2(OH)\}ClO_4$ are much more stable than those of $[Mn(OEP)]_2O$.

The synthesis and crystallization of $[Mn(OEP)(H_2O)]ClO_4$ are straightforward. Relatively dilute $HClO_4$ must be used to avoid significant demetalation of the manganese porphyrin. As in the iron case,[29] the $\pi-\pi$-interacting pair of porphyrin rings inhibits the coordination of a second water molecule and the formation of the six-coordinate diaquo complex. However, it should also be noted that the aquo ligand will be replaced by the perchlorate anion if recrystallization is performed with carefully dried solvents. A similar phenomenon has been observed in the iron system where recrystallization of $[Fe(OEP)(H_2O)]ClO_4$ under rigorously dry conditions leads to triclinic, crystalline $[Fe(OEP)(OClO_3)]$.[33]

Structures. The structural parameters ($Mn-N_p$ distances and manganese atom displacement) of $[Mn(OEP)(H_2O)]ClO_4$ are typical of five-coordinate, high-spin manganese(III) porphyrins.[34-43] The axial $Mn-O(H_2O)$ bond distance is 2.149(3) Å, very close to the 2.145(5)-Å value reported for benzene-solvated $[Mn(TPP)(H_2O)]^+$ [38] and longer than the 2.105(4)-Å value reported for unsolvated $[Mn(TPP)(H_2O)]^+$.[39] Hill and co-workers[38] attributed the differences in the axial bond distances to the effects of a π complex between the aquomanganese(III) porphyrinate and an aromatic solvent molecule, which was presumed to act as an additional ligand with no

Table 5. Bond Lengths (Å) for $\{[Mn(OEP)]_2OH\}ClO_4 \cdot 3CH_2Cl_2$[a]

Mn(1)−O(1)	1.998(2)	Mn(2)−O(1)	2.024(2)
Mn(1)−1N(1)	1.999(2)	Mn(2)−2N(1)	2.005(2)
Mn(1)−1N(2)	2.009(2)	Mn(2)−2N(2)	2.003(2)
Mn(1)−1N(3)	2.012(2)	Mn(2)−2N(3)	2.015(2)
Mn(1)−1N(4)	2.003(2)	Mn(2)−2N(4)	2.004(2)
1N(1)−1C(a1)	1.377(3)	2N(1)−2C(a1)	1.380(3)
1N(1)−1C(a2)	1.379(3)	2N(1)−2C(a2)	1.378(3)
1N(2)−1C(a3)	1.377(3)	2N(2)−2C(a3)	1.374(3)
1N(2)−1C(a4)	1.378(3)	2N(2)−2C(a4)	1.375(3)
1N(3)−1C(a5)	1.380(3)	2N(3)−2C(a5)	1.373(3)
1N(3)−1C(a6)	1.372(3)	2N(3)−2C(a6)	1.381(3)
1N(4)−1C(a7)	1.380(3)	2N(4)−2C(a7)	1.380(3)
1N(4)−1C(a8)	1.372(3)	2N(4)−2C(a8)	1.380(3)
1C(a1)−1C(b1)	1.438(4)	2C(a1)−2C(b1)	1.442(4)
1C(a2)−1C(b2)	1.435(4)	2C(a2)−2C(b2)	1.437(4)
1C(a3)−1C(b3)	1.444(3)	2C(a3)−2C(b3)	1.441(3)
1C(a4)−1C(b4)	1.441(4)	2C(a4)−2C(b4)	1.443(4)
1C(a5)−1C(b5)	1.443(4)	2C(a5)−2C(b5)	1.441(4)
1C(a6)−1C(b6)	1.441(4)	2C(a6)−2C(b6)	1.435(4)
1C(a7)−1C(b7)	1.443(4)	2C(a7)−2C(b7)	1.437(4)
1C(a8)−1C(b8)	1.441(4)	2C(a8)−2C(b8)	1.439(3)
1C(a1)−1C(m1)	1.387(4)	2C(a1)−2C(m1)	1.383(4)
1C(a2)−1C(m2)	1.383(4)	2C(a2)−2C(m2)	1.385(4)
1C(a3)−1C(m2)	1.380(4)	2C(a3)−2C(m2)	1.380(4)
1C(a4)−1C(m3)	1.378(4)	2C(a4)−2C(m3)	1.375(4)
1C(a5)−1C(m3)	1.377(4)	2C(a5)−2C(m3)	1.385(4)
1C(a6)−1C(m4)	1.386(4)	2C(a6)−2C(m4)	1.380(4)
1C(a7)−1C(m4)	1.377(4)	2C(a7)−2C(m4)	1.381(4)
1C(a8)−1C(m1)	1.384(4)	2C(a8)−2C(m1)	1.376(4)
1C(b1)−1C(b2)	1.361(4)	2C(b1)−2C(b2)	1.359(4)
1C(b3)−1C(b4)	1.363(4)	2C(b3)−2C(b4)	1.353(4)
1C(b5)−1C(b6)	1.360(4)	2C(b5)−2C(b6)	1.362(4)
1C(b7)−1C(b8)	1.358(4)	2C(b7)−2C(b8)	1.363(4)
1C(b1)−1C(11)	1.492(4)	2C(b1)−2C(11)	1.498(4)
1C(b2)−1C(21)	1.504(4)	2C(b2)−2C(21)	1.499(4)
1C(b3)−1C(31)	1.492(4)	2C(b3)−2C(31)	1.500(4)
1C(b4)−1C(41)	1.496(4)	2C(b4)−2C(41)	1.499(4)
1C(b5)−1C(51)	1.497(4)	2C(b5)−2C(51)	1.495(4)
1C(b6)−1C(61)	1.501(4)	2C(b6)−2C(61)	1.498(4)
1C(b7)−1C(71)	1.499(4)	2C(b7)−2C(71)	1.496(4)
1C(b8)−1C(81)	1.497(4)	2C(b8)−2C(81)	1.494(4)
1C(11)−1C(12)	1.523(5)	2C(11)−2C(12)	1.527(4)
1C(21)−1C(22)	1.525(5)	2C(21)−2C(22)	1.524(4)
1C(31)−1C(32)	1.522(4)	2C(31)−2C(32)	1.523(4)
1C(41)−1C(42)	1.532(4)	2C(41)−2C(42)	1.529(4)
1C(51)−1C(52)	1.521(4)	2C(51)−2C(52)	1.529(4)
1C(61)−1C(62)	1.514(6)	2C(61)−2C(62)	1.520(5)
1C(71)−1C(72)	1.525(4)	2C(71)−2C(72)	1.521(4)
1C(81)−1C(82)	1.523(5)	2C(81)−2C(82)	1.525(5)
O(1)−H	0.74(5)	C(2a)−Cl(5a)	1.79(2)
Cl(1a)−O(2)	1.379(5)	C(2a)−Cl(5b)	1.721(12)
Cl(1a)−O(3)	1.404(4)	C(2b)−Cl(4)	1.64(2)
Cl(1a)−O(4a)	1.415(6)	C(2b)−Cl(5a)	1.96(2)
Cl(1a)−O(5a)	1.439(5)	C(2b)−Cl(5b)	1.61(2)
Cl(1b)−O(2)	1.526(6)	C(3)−Cl(6)	1.72(2)
Cl(1b)−O(3)	1.448(6)	C(3)−Cl(7)	1.70(2)
Cl(1b)−O(4b)	1.413(9)	C(4)−Cl(8)	1.83(2)
Cl(1b)−O(5b)	1.438(10)	C(4)−Cl(9)	1.71(2)
C(1)−Cl(2)	1.754(4)	C(5)−Cl(10)	1.73(2)
C(1)−Cl(3)	1.758(5)	C(5)−Cl(11)	1.72(2)
C(2a)−Cl(4)	1.674(11)		

[a] Estimated standard deviations of the least significant digits are given in parentheses.

(33) Cheng, B.; Debrunner, P. G.; Scheidt, W. R. Work in Progress.
(34) Day, V. W.; Stults, B. R.; Tasset, E. L.; Marianelli, R. S.; Boucher, L. J. *Inorg. Nucl. Chem. Lett.* **1975**, *11*, 505.
(35) Tulinsky, A.; Chen, B. M. L. *J. Am. Chem. Soc.* **1977**, *99*, 3647.
(36) Anderson, O. P.; Lavallee, D. K. *Inorg. Chem.* **1977**, *16*, 1634.
(37) Scheidt, W. R.; Lee, Y. J.; Luangdilok, W.; Haller, K. J.; Anzai, K.; Hatano, K. *Inorg. Chem.* **1983**, *22*, 1516.
(38) Williamson, M. M.; Hill, C. L. *Inorg. Chem.* **1987**, *26*, 4155.
(39) Williamson, M. M.; Hill, C. L. *Inorg. Chem.* **1986**, *25*, 4668.
(40) Jinghe, Z.; Shongchun, J.; Zhungsheng, J.; Rizhen, J. *Chin. J. Appl. Chem.* **1988**, *5*, 50.
(41) Suslick, K. S.; Watson, R. A. *Inorg. Chem.* **1991**, *30*, 912.
(42) Suslick, K. S.; Watson, R. A.; Wilson, S. R. *Inorg. Chem.* **1991**, *30*, 2311.
(43) Armstrong, R. S.; Foran, G. J.; Hambley, T. W. *Acta Crystallogr., Sect. C* **1993**, *C49*, 236.

Table 6. Bond Angles (deg) for $\{[Mn(OEP)]_2OH\}ClO_4 \cdot 3CH_2Cl_2$[a]

O(1)−Mn(1)−1N(1)	97.70(9)	O(1)−Mn(2)−2N(1)	106.55(9)	1C(b1)−1C(b2)−1C(a2)	107.4(2)	2C(b1)−2C(b2)−2C(a2)	107.1(2)
O(1)−Mn(1)−1N(2)	98.88(9)	O(1)−Mn(2)−2N(2)	94.35(9)	1C(b4)−1C(b3)−1C(a3)	106.6(2)	2C(b4)−2C(b3)−2C(a3)	106.6(2)
O(1)−Mn(1)−1N(3)	94.20(9)	O(1)−Mn(2)−2N(3)	86.15(9)	1C(b3)−1C(b4)−1C(a4)	107.0(2)	2C(b3)−2C(b4)−2C(a4)	107.2(2)
O(1)−Mn(1)−1N(4)	94.72(9)	O(1)−Mn(2)−2N(4)	96.64(9)	1C(b6)−1C(b5)−1C(a5)	106.6(2)	2C(b6)−2C(b5)−2C(a5)	106.7(2)
1N(1)−Mn(1)−1N(2)	89.52(9)	2N(1)−Mn(2)−2N(2)	89.41(9)	1C(b5)−1C(b6)−1C(a6)	107.0(2)	2C(b5)−2C(b6)−2C(a6)	106.9(2)
1N(1)−Mn(1)−1N(3)	168.08(9)	2N(1)−Mn(2)−2N(3)	167.29(9)	1C(b8)−1C(b7)−1C(a7)	106.8(2)	2C(b8)−2C(b7)−2C(a7)	107.0(2)
1N(1)−Mn(1)−1N(4)	89.46(9)	2N(1)−Mn(2)−2N(4)	88.98(9)	1C(b7)−1C(b8)−1C(a8)	106.8(2)	2C(b7)−2C(b8)−2C(a8)	106.6(2)
1N(2)−Mn(1)−1N(3)	89.15(9)	2N(2)−Mn(2)−2N(3)	89.58(9)	1C(a1)−1C(b1)−1C(11)	124.7(2)	2C(a1)−2C(b1)−2C(11)	124.9(2)
1N(2)−Mn(1)−1N(4)	166.38(9)	2N(2)−Mn(2)−2N(4)	168.90(9)	1C(a2)−1C(b2)−1C(21)	124.3(2)	2C(a2)−2C(b2)−2C(21)	124.7(2)
1N(3)−Mn(1)−1N(4)	89.04(9)	2N(3)−Mn(2)−2N(4)	89.57(9)	1C(a3)−1C(b3)−1C(31)	125.0(2)	2C(a3)−2C(b3)−2C(31)	125.3(3)
1C(a1)−1N(1)−Mn(1)	126.1(2)	2C(a1)−2N(1)−Mn(2)	128.0(2)	1C(a4)−1C(b4)−1C(41)	124.6(2)	2C(a4)−2C(b4)−2C(41)	124.4(2)
1C(a2)−1N(1)−Mn(1)	127.7(2)	2C(a2)−2N(1)−Mn(2)	126.9(2)	1C(a5)−1C(b5)−1C(51)	125.4(3)	2C(a5)−2C(b5)−2C(51)	124.3(2)
1C(a3)−1N(2)−Mn(1)	127.4(2)	2C(a3)−2N(2)−Mn(2)	126.5(2)	1C(a6)−1C(b6)−1C(61)	124.9(3)	2C(a6)−2C(b6)−2C(61)	124.2(3)
1C(a4)−1N(2)−Mn(1)	126.4(2)	2C(a4)−2N(2)−Mn(2)	126.8(2)	1C(a7)−1C(b7)−1C(71)	124.4(2)	2C(a7)−2C(b7)−2C(71)	124.9(2)
1C(a5)−1N(3)−Mn(1)	125.8(2)	2C(a5)−2N(3)−Mn(2)	126.9(2)	1C(a8)−1C(b8)−1C(81)	124.5(2)	2C(a8)−2C(b8)−2C(81)	124.8(2)
1C(a6)−1N(3)−Mn(1)	127.8(2)	2C(a6)−2N(3)−Mn(2)	125.6(2)	1C(b2)−1C(b1)−1C(11)	128.7(3)	2C(b2)−2C(b1)−2C(11)	128.5(2)
1C(a7)−1N(4)−Mn(1)	127.9(2)	2C(a7)−2N(4)−Mn(2)	126.3(2)	1C(b1)−1C(b2)−1C(21)	128.1(2)	2C(b1)−2C(b2)−2C(21)	128.1(2)
1C(a8)−1N(4)−Mn(1)	125.6(2)	2C(a8)−2N(4)−Mn(2)	127.8(2)	1C(b4)−1C(b3)−1C(31)	128.4(2)	2C(b4)−2C(b3)−2C(31)	128.2(2)
1C(a1)−1N(1)−1C(a2)	106.0(2)	2C(a1)−2N(1)−2C(a2)	105.2(2)	1C(b3)−1C(b4)−1C(41)	128.2(2)	2C(b3)−2C(b4)−2C(41)	128.3(2)
1C(a3)−1N(2)−1C(a4)	105.8(2)	2C(a3)−2N(2)−2C(a4)	105.6(2)	1C(b6)−1C(b5)−1C(51)	128.0(3)	2C(b6)−2C(b5)−2C(51)	128.8(3)
1C(a5)−1N(3)−1C(a6)	105.7(2)	2C(a5)−2N(3)−2C(a6)	105.5(2)	1C(b5)−1C(b6)−1C(61)	128.1(3)	2C(b5)−2C(b6)−2C(61)	128.7(3)
1C(a7)−1N(4)−1C(a8)	105.5(2)	2C(a7)−2N(4)−2C(a8)	105.4(2)	1C(b8)−1C(b7)−1C(71)	128.8(2)	2C(b8)−2C(b7)−2C(71)	128.1(2)
1N(1)−1C(a1)−1C(b1)	110.2(2)	2N(1)−2C(a1)−2C(b1)	110.6(2)	1C(b7)−1C(b8)−1C(81)	128.7(3)	2C(b7)−2C(b8)−2C(81)	128.5(2)
1N(1)−1C(a2)−1C(b2)	109.7(2)	2N(1)−2C(a2)−2C(b2)	110.6(2)	1C(a1)−1C(m1)−1C(a8)	125.1(2)	2C(a1)−2C(m1)−2C(a8)	125.2(2)
1N(2)−1C(a3)−1C(b3)	110.3(2)	2N(2)−2C(a3)−2C(b3)	110.6(2)	1C(a2)−1C(m2)−1C(a3)	125.4(2)	2C(a2)−2C(m2)−2C(a3)	125.4(2)
1N(2)−1C(a4)−1C(b4)	110.2(2)	2N(2)−2C(a4)−2C(b4)	110.0(2)	1C(a4)−1C(m3)−1C(a5)	125.7(2)	2C(a4)−2C(m3)−2C(a5)	125.8(2)
1N(3)−1C(a5)−1C(b5)	110.3(2)	2N(3)−2C(a5)−2C(b5)	110.6(2)	1C(a6)−1C(m4)−1C(a7)	125.4(3)	2C(a6)−2C(m4)−2C(a7)	125.8(2)
1N(3)−1C(a6)−1C(b6)	110.3(2)	2N(3)−2C(a6)−2C(b6)	110.4(2)	1C(b1)−1C11)−1C(12)	113.4(2)	2C(b1)−2C(11)−2C(12)	111.9(2)
1N(4)−1C(a7)−1C(b7)	110.2(2)	2N(4)−2C(a7)−2C(b7)	110.4(2)	1C(b2)−1C21)−1C(22)	112.2(3)	2C(b2)−2C(21)−2C(22)	113.0(2)
1N(4)−1C(a8)−1C(b8)	110.6(2)	2N(4)−2C(a8)−2C(b8)	110.6(2)	1C(b3)−1C31)−1C(32)	112.1(2)	2C(b3)−2C(31)−2C(32)	113.5(2)
1N(1)−1C(a1)−1C(m1)	124.6(2)	2N(1)−2C(a1)−2C(m1)	124.7(2)	1C(b4)−1C41)−1C(42)	112.2(2)	2C(b4)−2C(41)−2C(42)	111.8(2)
1N(1)−1C(a2)−1C(m2)	124.9(2)	2N(1)−2C(a2)−2C(m2)	124.6(2)	1C(b5)−1C51)−1C(52)	113.3(3)	2C(b5)−2C(51)−2C(52)	112.0(2)
1N(2)−1C(a3)−1C(m2)	125.0(2)	2N(2)−2C(a3)−2C(m2)	124.7(2)	1C(b6)−1C61)−1C(62)	112.5(3)	2C(b6)−2C(61)−2C(62)	112.1(3)
1N(2)−1C(a4)−1C(m3)	124.8(2)	2N(2)−2C(a4)−2C(m3)	125.2(2)	1C(b7)−1C71)−1C(72)	112.4(2)	2C(b7)−2C(71)−2C(72)	112.2(2)
1N(3)−1C(a5)−1C(m3)	124.7(2)	2N(3)−2C(a5)−2C(m3)	124.4(2)	1C(b8)−1C81)−1C(82)	112.7(2)	2C(b8)−2C(81)−2C(82)	111.8(3)
1N(3)−1C(a6)−1C(m4)	124.8(2)	2N(3)−2C(a6)−2C(m4)	124.9(2)	Mn(1)−O(1)−H	104(4)	Mn(2)−O(1)−H	103(4)
1N(4)−1C(a7)−1C(m4)	124.8(2)	2N(4)−2C(a7)−2C(m4)	124.8(2)	Mn(1)−O(1)−Mn(2)	152.73(11)	O(3)−Cl(1b)−O(5b)	101.6(5)
1N(4)−1C(a8)−1C(m1)	124.9(2)	2N(4)−2C(a8)−2C(m1)	124.8(2)	O(2)−Cl(1a)−O(3)	114.2(3)	O(4b)−Cl(1b)−O(5b)	110.0(7)
1C(m1)−1C(a1)−1C(b1)	125.0(2)	2C(m1)−2C(a1)−2C(b1)	124.6(2)	O(2)−Cl(1a)−O(4a)	111.0(3)	Cl(2)−C(1)−Cl(3)	111.5(2)
1C(m2)−1C(a2)−1C(b2)	125.3(2)	2C(m2)−2C(a2)−2C(b2)	124.8(2)	O92)−Cl(1a)−O(5a)	107.2(4)	Cl(4)−C(2a)−Cl(5a)	99.0(7)
1C(m2)−1C(a3)−1C(b3)	124.7(2)	2C(m2)−2C(a3)−2C(b3)	124.7(2)	O(3)−Cl(1a)−O(4a)	107.1(3)	Cl(4)−C(2a)−Cl(5b)	117.0(8)
1C(m3)−1C(a4)−1C(b4)	125.0(2)	2C(m3)−2C(a4)−2C(b4)	124.7(2)	O(3)−Cl(1a)−O(5a)	109.0(4)	Cl(4)−C(2b)−Cl(5b)	126.4(13)
1C(m3)−1C(a5)−1C(b5)	124.8(2)	2C(m3)−2C(a5)−2C(b5)	124.9(2)	O(4a)−Cl(1a)−O(5a)	108.3(5)	Cl(4)−C(2b)−Cl(5a)	93.7(10)
1C(m4)−1C(a6)−1C(b6)	124.8(3)	2C(m4)−2C(a6)−2C(b6)	124.7(2)	O(2)−Cl(1b)−O(3)	103.5(3)	Cl(6)−C(3)−Cl(7)	115.0(11)
1C(m4)−1C(a7)−1C(b7)	124.8(3)	2C(m4)−2C(a7)−2C(b7)	124.7(2)	O(2)−Cl(1b)−O(4b)	111.8(5)	Cl(8)−C(4)−Cl(9)	111.3(8)
1C(m1)−1C(a8)−1C(b8)	124.3(2)	2C(m1)−2C(a8)−2C(b8)	124.6(2)	O(2)−Cl(1b)−O(5b)	110.9(5)	Cl(10)−C(5)−Cl(11)	108.2(13)
1C(b2)−1C(b1)−1C(a1)	106.5(2)	2C(b2)−2C(b1)−2C(a1)	106.5(2)	O(3)−Cl(1b)−O(4b)	118.5(5)		

[a] Estimated standard deviations of the least significant digits are given in parentheses.

specific orbital interaction between the manganese ion and the benzene. In $[Mn(OEP)(H_2O)]ClO_4$, an adjacent metalloporphyrin cation interacts to form a porphyrin···porphyrin π complex as described under Results. The interaction between the manganese(III) ion and the adjacent aromatic (porphyrin) entity must be regarded as a nonspecific one leading to an increase in the axial bond distance. Finally, it is to be noted that the interporphyrin interactions are similar to those observed for $[Fe(OEP)(H_2O)]ClO_4 \cdot 2H_2O$[29] and numerous other derivatives.[28]

The average Mn−N_p bond distance (2.006(5) Å) and manganese atom displacement from the 24-atom mean plane (0.21 Å) in $\{[Mn(OEP)]_2(OH)\}ClO_4$ are within the range expected for high-spin five-coordinate manganese(III) porphyrinates. The identity of the bridging axial ligand as a hydroxide ion is clearly defined by the stoichiometry established by the crystal structure and the definite location and least-squares behavior of the hydrogen atom in the X-ray structure determination. The average axial Mn−O(OH$^-$) bond distance of 2.011 Å is also clearly consistent with an anionic ligand and not a neutral ligand. Moreover, the distances are much longer than the 1.78−1.84 Å expected for a bridging oxo ligand.

There are a number of interesting features concerning the two porphyrin rings and the inter-ring interactions of $\{[Mn(OEP)]_2$-

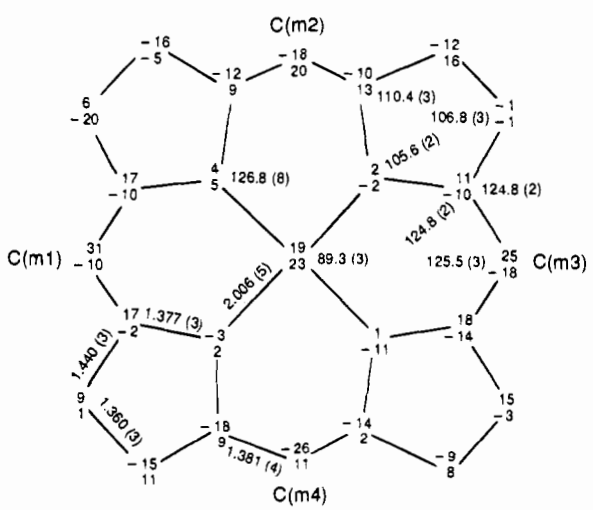

Figure 5. Formal diagram of the porphinato core of $\{[Mn(OEP)]_2$-$(OH)\}ClO_4$, displaying the average values for the bond parameters. Values for the perpendicular displacements of each atom (in units of 0.01 Å) of the 24-atom core of both rings are shown; the upper value of the pair is for ring 1 while the lower value is for ring 2. For both rings, a positive value is a displacement toward the other ring of the dimer.

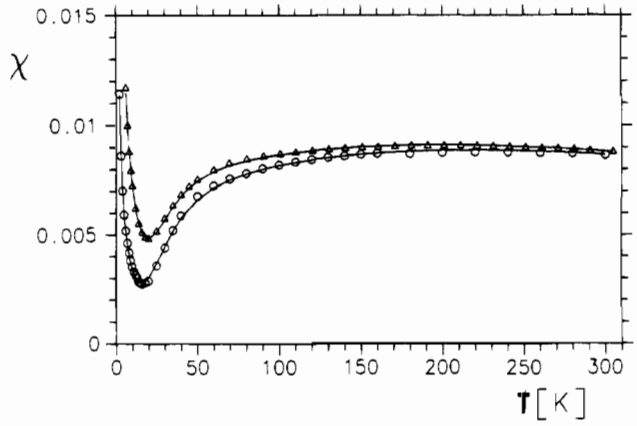

Figure 6. Temperature dependence of the magnetic susceptibility of two different samples of $\{[Mn(OEP)]_2(OH)\}ClO_4$: (○) sample 1; (△) sample 2. The solid lines were calculated with the following sets of parameters: $J = -35.6\ cm^{-1}$, $D = -9.7\ cm^{-1}$ (sample 1); $J = -35.3\ cm^{-1}$, $D = -7.0\ cm^{-1}$ (sample 2). The mole fraction of a monomeric impurity with a ZFS equal to $-2.3\ cm^{-1}$ was adjusted to $w_{mo} = 1.0\%$ for sample 1 and to $w_{mo} = 2.4\%$ for sample 2.

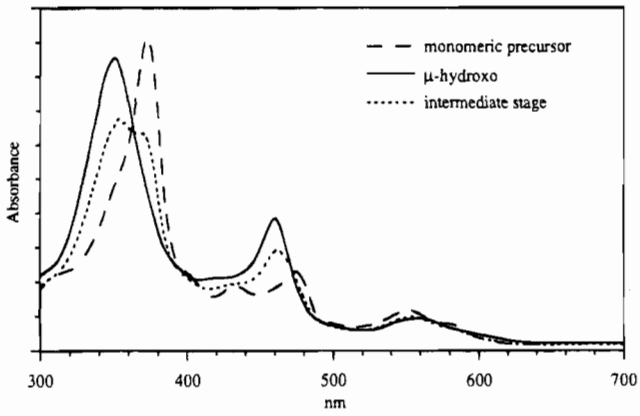

Figure 7. Electronic spectra monitoring the synthesis of $\{[Mn(OEP)]_2(OH)\}ClO_4$ from $[Mn(OEP)(H_2O)]ClO_4$. Concentrations of all species are arbitrary and were chosen to emphasize the shifts in the spectra.

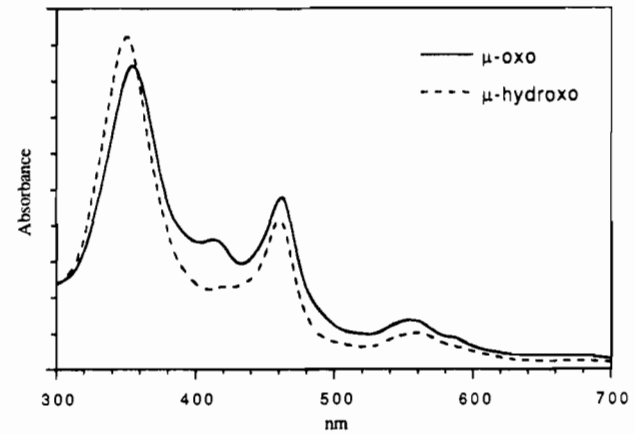

Figure 8. Electronic spectra of $\{[Mn(OEP)]_2(OH)\}ClO_4$ and the product resulting from an attempted deprotonation. The concentrations of the manganese porphyrin in the two spectra are effectively equal.

$(OH)\}ClO_4$ that call for attention. The 152.73° value for the Mn(1)−O−Mn(2) bridge angle is substantially larger than expected for a bridging hydroxide ligand.[44] This bridge angle would require a dihedral angle of 27° between the two porphinato cores if both axial Mn−O vectors were normal to their respective porphyrin cores. However, the dihedral angle between the two 24-atom mean planes is only 12.7° while the value between the two N_4 mean planes is 15.5°. These observed dihedral angles suggest a significant interaction between the two porphyrin rings. Finally and most strikingly, the two porphyrin units within a molecule have a nearly eclipsed inter-ring orientation with an average N−Mn−Mn′−N′ dihedral angle of 4.3°. The closest pair of pyrrole rings (N(1)'s) approach each other to within about 3.4 Å; the closest C···C contact between these pyrrole rings is ~3.5 Å between β-carbon atoms (see Figure 3). In addition, the methylene carbon atom pairs of these pyrroles make 3.6 Å contacts with each other. At the two N(1) pyrroles, the porphyrin rings are clearly rather crowded. Part of the inter-ring congestion is minimized by the strongly asymmetric bond angles subtended at Mn(2); the two angles O−Mn(2)−2N(1) and O−Mn(2)−2N(3) of 106.55(9) and 86.15(9)° allow the smaller observed dihedral angle between the two cores. The two cores display substantial S_4 ruffling (Figure 5). However, the two closest pyrrole ring planes are nearly parallel, which thus relieves some of the inter-ring strain. As seen in Figure 3, the four closest inter-ring peripheral ethyl groups on each porphyrin ring point away from each other in what can be termed the "up" position. The remaining four ethyl groups on one porphyrin ring are also up, while on the other ring the groups are in a four up/four down orientation. It is this porphyrin ring that closely approaches the analogous ring of another $\{[Mn(OEP)]_2(OH)\}ClO_4$ molecule with an interplanar spacing of 3.33 Å and a lateral shift of 3.51 Å.

We believe that the observed, nearly eclipsed inter-ring orientation of the porphyrin rings in $\{[Mn(OEP)]_2(OH)\}ClO_4$ primarily results from peripheral ethyl group interactions. We recently determined[45] the molecular structure and carried out molecular mechanics calculations for two crystalline forms of $[Fe(OEP)]_2O$, where the inter-ring orientations are ~17°. In that system, molecular mechanics calculations support the idea that the peripheral group interactions drive the observed, near-eclipsed inter-ring orientations.

Several of these interesting structural features of $\{[Mn(OEP)]_2(OH)\}ClO_4$ are very similar to those observed for the μ-hydroxo iron complex.[12] The Mn(1)−O−Mn(2) bridge angle is slightly larger than that observed in $\{[Fe(OEP)]_2(OH)\}ClO_4$ (146.2(2)°); the pyrrole rings are also nearly eclipsed in the latter complex (average N−Fe−Fe′−N′ = 8.4°). A similar asymmetry in the range of $O-M-N_p$ bond angles is also observed in the iron species, which is presumed to serve the same role of relieving some inter-ring strain.

Dinuclear manganese systems are commonly found to have multiple bridging ligand sets, including bis(μ-hydroxo),[46] bis(μ-oxo),[46,47] tris(μ-oxo),[47a] tribridging oxo dicarboxylate,[48] and others.[49] Dinuclear manganese complexes supported by a single bridging ligand appear to be extremely rare; only four structurally characterized systems with a single bridge (all oxo) are known to us.[50-53] This is in distinct contrast to the case of complexes formed by the manganese close neighbor iron, where

(44) Expected value for μ-hydroxo angle—typically smaller than that for the analogous system with μ-oxo; the range of values is 105−110°.

(45) Cheng, B.; Hobbs, J. D.; Debrunner, P. G.; Erlebacher, J.; Shelnutt, J. A.; Scheidt, W. R. *Inorg. Chem.* **1995**, *34*, 102.

(46) Kitajima, N.; Singh, U. P.; Amagai, H.; Osawa, M.; Moro-oka, Y. *J. Am. Chem. Soc.* **1991**, *113*, 7757.

(47) (a) Wieghardt, K.; Bossek, U.; Nuber, B.; Weiss, J.; Bonvoisin, J.; Corbella, M.; Vitols, S. E.; Girerd, J. J. *J. Am. Chem. Soc.* **1988**, *110*, 7398. (b) Gohdes, J. W.; Armstrong, W. H. *Inorg. Chem.* **1992**, *31*, 368. (c) Larson, E. J.; Lah, M. S.; Li, X.; Bonadies, J. A.; Pecoraro, V. L. *Inorg. Chem.* **1992**, *31*, 373.

(48) Sheats, J. E.; Czernuszewicz, R. S.; Dismukes, G. C.; Rheingold, A. L.; Petrouleas, V.; Stubbe, J.; Armstrong, W. H.; Beer, R. H.; Lippard, S. J. *J. Am. Chem. Soc.* **1987**, *109*, 1435.

(49) A thorough listing of bridging types and investigations has been given by Que and True.[3] See Table VIII therein.

many more singly bridged species are known. Obviously, {-[Mn(OEP)]$_2$(OH)}ClO$_4$ is the first characterized manganese complex that contains a single hydroxide bridge. An apparent common feature of the four singly-bridged manganese systems is that the nonbridging ligands sterically hinder significantly the approach of additional bridging ligands to the manganese. The Mn−O−Mn bond angle is nearly linear in the four μ-oxo structures, with the smallest value equal to 168.4°.[52] The structural features of {[Mn(OEP)]$_2$(OH)}ClO$_4$ are entirely consistent with these steric requirements.

To our knowledge, there are only three previously characterized multinuclear manganese complexes with a bridging hydroxide ligand;[46,47] all contain multiple bridges and none are for a manganese(III) derivative.[54]

The hydroxide ion in {[Mn(OEP)]$_2$(OH)}ClO$_4$ is in a very unusual chemical environment. The only close contacts involving either the oxygen or hydrogen atom of the hydroxide ion are with atoms of the porphyrin rings. Although reasonably close contact between the hydroxide and the perchlorate ions might have been expected, the closest contact is a O(1)···O(3) distance of >6.5 Å. The distance between this perchlorate oxygen atom and the hydrogen is longer still. However, the hydroxide hydrogen atom is within hydrogen-bonding distance of the porphyrin nitrogen atom 2N(3) at 2.44 Å; the 2N(3)−H−O(1) angle of 108.1° is unusual for a hydrogen bond.

Magnetic Properties. The temperature dependence of the magnetic susceptibility of {[Mn(OEP)]$_2$(OH)}ClO$_4$ is fitted well by assuming that the bridging hydroxo ligand mediates a moderately strong antiferromagnetic exchange ($J = -35.5 \pm 0.2$ cm^{-1}) between the two $S = 2$ Mn(III) centers. In comparison, the single bridging oxo ligand in a binuclear Mn(III) Schiff base complex results in a much stronger coupling ($J = -120$ cm^{-1}).[52] While the two complexes have similar bridging structures and presumably use an analogous exchange pathway, the differences in structure—a more nearly linear Mn−O−Mn bridge angle (168.4° vs 152.73°) and shorter axial bridge distances (1.754 Å vs 2.011 Å) in the oxo-bridged complex—would favor stronger antiferromagnetic coupling for it. Nonetheless, the magnitude of the antiferromagnetic coupling in the hydroxide complex is unprecedentedly large. The only direct hydroxo-bridged manganese comparisons to be made are with a μ-hydroxo bis(μ-acetato) dimanganese(II) complex[55] and two Mn(IV) tetramers[56] where the coupling mediated by hydroxide is $J = -9$ and -20 to 22 cm^{-1}, respectively. The differences in coupling constant are consistent with the idea that stronger antiferromagnetic coupling if found as the M−O−M bridge angle becomes larger.[57] It should be noted that the solution susceptibility value measured by NMR methods in $CDCl_3$ corresponds[58] to an antiferromagnetic coupling constant J of -31.7 cm^{-1}, in satisfactory agreement with the results from solid-state measurements.

The rather large absolute value of the zero-field-splitting term ($D = -8 \pm 2$ cm^{-1}) for the {[Mn(OEP)]$_2$(OH)}ClO$_4$ complex is at first sight surprising, in view of the range found (-1 to -3 cm^{-1}) for the limited number of mononuclear Mn(III) porphyrins that have been investigated so far.[26,30] It is well-known that for a constant porphyrin the D values depend on the nature of axial ligand[26] and that weaker axial ligation results in a larger absolute value of D; but since the influence of an axial hydroxo ligand on the ZFS is not documented, the above result should be accepted with some caution. One can note, however, that several cases were reported very recently in which Mn(III) complexes exhibit D values ≈ -8 cm^{-1}.[59] Thus, in the case of {[Mn(OEP)]$_2$(OH)}ClO$_4$, a similar value of the ZFS is not unreasonable. Furthermore, the location of the bridging hydroxide off the C_4 axes of the two porphyrins presumably introduces some rhombic distortion in the dimer, but we have not included an E term in the spin Hamiltonian in order to limit the number of adjustable parameters. As a result, the value of the adjusted D term could contain the hidden contribution of a rhombic distortion.

Summary. The synthesis of the novel hydroxo-bridged complex {[Mn(OEP)]$_2$(OH)}ClO$_4$ from mononuclear or dinuclear manganese(III) complexes is described. The X-ray structure shows that each Mn(III) ion is axially coordinated with an Mn−O(H)−Mn bridge angle of 152.73(11)°. The two porphyrin cores of the binuclear species are nearly eclipsed. The Mn(III)···Mn(III) exchange interaction in the hydroxo-bridged complex {[Mn(OEP)]$_2$(OH)}ClO$_4$ is moderately antiferromagnetic ($J = -35.5 \pm 0.2$ cm^{-1}) and modulated by zero-field-splitting effects, as in several other recently investigated systems.[31] The value of the ZFS, which is higher than usual, probably reflects weaker axial interaction and/or rhombic distortion.

Acknowledgment. We thank the National Institutes of Health for support of this research under Grant GM-38401 to W.R.S. Funding for the purchase of the FAST area detector diffractometer was provided through NIH Grant RR-06709. We thank Jean-Jacques Girerd and Jean-Marc Latour for helpful discussions.

Appendix

1. Theoretical Magnetic Susceptibilities of Two Exchange-Coupled Spins in Anisotropic Axial Environments. First, consider the mononuclear Mn(III) complex. The Mn(III) ion is located on the C_4 axis of the porphyrin ligand with a small out-of-plane displacement. The oxygen atom of the aquo ligand is also approximately on this axis. Thus, the $S = 2$, trivalent manganese ion is in a nearly axial environment. Choose a mononuclear direct reference frame $(O_i,\hat{i}_i\hat{j}_i,\hat{k}_i)$ centered at the Mn(III) ion i with the C_4 axis as the Z_i axis. In this frame, the simplest zero-field-splitting (ZFS) Hamiltonian is used for

(50) [Mn(TPP)(N$_3$)]$_2$O: Schardt, B. C.; Hollander, F. J.; Hill, C. L. *J. Am. Chem. Soc.* **1982**, *104*, 3964.
(51) [Mn(Pc)(Py)]]$_2$O: Vogt, L. H.; Zalkin, A.; Templeton, D. H. *Inorg. Chem.* **1967**, *6*, 1725.
(52) [Mn$_2$O(5-NO$_2$saldien)$_2$]: Kipke, C. A.; Scott, M. J.; Gohdes, J. W.; Armstrong, W. H. *Inorg. Chem.* **1990**, *29*, 2193.
(53) Mn$_2$C$_{54}$H$_{90}$N$_{12}$O$_3$B$_2$: Kitajima, N.; Osawa, M.; Tanaka, M.; Moro-oka, Y. *J. Am. Chem. Soc.* **1991**, *113*, 8952. This complex has two alkoxy-substituted tris(pyrazolyl)borate ligands.
(54) A claimed bis(μ-hydroxo)dimaganese(III) complex is most likely a bis(μ-oxo)dimaganese(IV) complex: Maslen, H. S.; Waters, T. N. *J. Chem. Soc., Chem. Commun.* **1973**, 760.
(55) Bossek, U.; Wieghardt, K.; Nuber, B.; Weiss, J. *Inorg. Chim. Acta* **1989**, *165*, 123.
(56) Hagen, K. S.; Westmoreland, T. D.; Scott, M. J.; Armstrong, W. H. *J. Am. Chem. Soc.* **1989**, *111*, 1907.
(57) Such a relationship for a bridging hydroxo has perhaps been best shown for copper(II) species: Hodgson, D. K. In *Progress in Inorganic Chemistry*; Lippard, S. J., Ed.; Interscience: New York, 1975; Vol. 19, Chapter 4. Although there are clearly potential limitations to comparing coupling constants for Mn complexes in different oxidations states, the Mn−O(H)−Mn angles are 109.4(3)° in the Mn(II) complex and 124.2(3)° in the Mn(IV) complex.
(58) In order to estimate the coupling constant J, a "one-parameter-fit" procedure was applied using the equation

$$\chi_A = \frac{3K}{T}\left[\frac{30 + 14x^8 + 5x^{14} + x^{18}}{9 + 7x^8 + 5x^{14} + 3x^{18} + x^{20}}\right]$$

where $x = \exp(-J/kT)$ and $K = Ng^2\beta^2/3k$. Of course, such a procedure is not guaranteed to produce a coupling constant J with sufficient reliability.
(59) Saadeh, S. M.; Trojan, K. L.; Kampf, J. W.; Hatfield, W. E.; Pecoraro, V. L. *Inorg. Chem.* **1993**, *32*, 3034.

modeling the energy spectrum of such an ion i. It is

$$\mathcal{H}_{fs}(i) = D[S_{iz}^2 - {}^1/_3 S_i(S_i + 1)] \quad \text{(A1)}$$

where the index "fs" stands for "fine structure" and D is the axial parameter of the ZFS tensor.[60]

Detailed EPR studies of Mn(III) in the strong, essentially octahedral, field of the six oxide ions of the rutile structure have shown that the values of the Zeeman $\tilde{g}$ factor are very nearly 2.[61] Furthermore, magnetic data for polycrystalline samples are rather insensitive to the anisotropy of the $\tilde{g}$ factor[62a] which will be set equal to $g = 2$. The Zeeman interaction is

$$\mathcal{H}_z(i) = \mu_B g \vec{H} \cdot \vec{S} \quad \text{(A2)}$$

where $\vec{H}$ is the external magnetic field.

Second, the total spin Hamiltonian of the Mn(III) dimer can be written as

$$\mathcal{H}_{tot} = \mathcal{H}(1) + \mathcal{H}(2) - 2J\vec{S}_1 \cdot \vec{S}_2 \quad \text{(A3a)}$$

where

$$\mathcal{H}(i) = \mathcal{H}_{fs}(i) + \mathcal{H}_z(i) \quad (i = 1, 2) \quad \text{(A3b)}$$

are the partial Hamiltonians associated with the interacting Mn(III) ions and $-2J\vec{S}_1 \cdot \vec{S}_2$ is their exchange interaction.

In order to diagonalize $\mathcal{H}_{tot}$, the mononuclear Hamiltonians should be expressed with respect to the same reference molecular frame $(O,\hat{i},\hat{j},\hat{k})$. Let $\mathcal{R}(i) = [\mathcal{R}(i)_{\alpha\beta}]$ ($\alpha, \beta = 1, 2, 3$) be the rotation which transforms the unit vectors of the molecular frame to those of the mononuclear reference frame $(O_i,\hat{i}_i,\hat{j}_i,\hat{k}_i)$. The fine structure Hamiltonians can be rewritten in terms of a second-rank irreducible tensor of operators[63] $T(S_i)_{2q}$. For any spin S these operators are defined as[64]

$$T(S)_{20} = \frac{N_2}{\sqrt{6}}[3S_z^2 - S(S+1)]$$

$$T(S)_{2\pm1} = \mp\frac{N_2}{2}[(S_xS_z + S_zS_x) \pm i(S_yS_z + S_zS_y)] \quad \text{(A4)}$$

$$T(S)_{2\pm2} = \frac{N_2}{2}[S_x^2 - S_y^2 \pm i(S_xS_y + S_yS_x)]$$

where

$$N_2 = \left[\frac{30}{(2S+3)(2S+1)S(2S-1)(S+1)}\right]^{1/2}$$

The fine structure Hamiltonians become

$$\mathcal{H}_{fs}(i) = f_0 T(S_i)_{20} \quad \text{(A5a)}$$

with

$$f_0 = \frac{\sqrt{6}}{3N_2}D \quad \text{(A5b)}$$

Let $R^{(2)}_{qp}(i)$ ($q, p = -2, \ldots, +2$) be the coefficients of the Wigner rotation matrix of order 2 associated with the active rotation[63] $\mathcal{R}(i) = [\mathcal{R}(i)_{\alpha\beta}]$. The rotation property of the tensor operators is

$$T(S_i)_{2p} = \sum_{q=-2}^{2} T(S_i)^{mol}_{2q} R^{(2)}_{qp}(i) \quad \text{(A6)}$$

where the $T(S_i)^{mol}_{2q}$ are the tensor operators which are built with the spin components in the molecular reference frame according to eq A4. Using eqs A5 and A6, the fine structure Hamiltonians can be rewritten in the molecular reference frame as

$$\mathcal{H}_{fs}(i) = f_0 \sum_{q=-2}^{2} R^{(2)}_{q0}(i)\, T(S_i)^{mol}_{2q} \quad \text{(A7)}$$

To sum up, the total spin Hamiltonian in the molecular reference frame, $\mathcal{H}_{tot}$, is defined by eq A3 where the fine structure parts $\mathcal{H}_{fs}(i)$ of the single-ion Hamiltonians $\mathcal{H}(i) = \mathcal{H}_{fs}(i) + \mathcal{H}_z(i)$ are given by eq A7.

Let H be the magnitude of the external magnetic field which is successively applied along the $\alpha = x, y, z$ directions of the molecular reference frame given by the unit vectors $\hat{u}_\alpha = \hat{i}, \hat{j}, \hat{k}$. The molar magnetization $M_A(H)_\alpha$ parallel to the magnetic field $\vec{H} = H\hat{u}_\alpha$ is given by

$$M_A(H)_\alpha = N_{Avog} m_{\|\alpha} \quad \text{(A8a)}$$

where $m_{\|\alpha}$ is the dimer magnetization parallel to the field. The dimer magnetization is calculated as the numerical derivative

$$m_{\|\alpha} = -\frac{\partial}{\partial H}\mathcal{F}[H\hat{u}_\alpha] \quad \text{(A8b)}$$

of the free energy[62b,65]

$$\mathcal{F}[H\hat{u}_\alpha] = -k_B T \ln\left\{\sum_n \exp\left[-\frac{E_n[H\hat{u}_\alpha]}{k_B T}\right]\right\} \quad \text{(A8c)}$$

where the E_n are the computed energy levels of the total spin Hamiltonian for the magnetic field $H\hat{u}_\alpha$. The molar magnetic susceptibility along the α direction is defined as

$$\chi_{\alpha\alpha} = \lim_{H\to 0} \frac{M_A(H)_\alpha}{H} \quad \text{(A9)}$$

Finally, the molar susceptibility of a crystal powder is given by

$$\chi = (\chi_{xx} + \chi_{yy} + \chi_{zz})/3 \quad \text{(A10)}$$

2. Monomeric Impurities among Dimer Crystallites. In a sample of randomly oriented dimer microcrystallites, let w_{mo} be the molar fraction of monomeric impurities. One mole of this sample is made of $N_{Avog}(1 - w_{mo})$ dimers and $N_{Avog}w_{mo}$ monomeric impurities. Its molar mass is

$$M = (1 - w_{mo})M_{di} + w_{mo}M_{mo}$$

where M_{di} and M_{mo} are the molar masses of the dimer and of the monomer, respectively. The susceptibility of an actual sample of mass M_{di}, which contains a mixture of $(M_{di}/M)N_{Avog}$ dimer and monomer molecules, is

(60) Abragam, A.; Bleaney, B. *Résonance Paramagnétique Electronique des Ions de Transition*; PUF: Paris, 1971; pp 139–170.
(61) Gerritsen, H. J.; Sabisky, E. S. *Phys. Rev.* **1963**, *132*, 1507.
(62) Kahn, O. *Molecular Magnetism*; VCH: Weinheim, Germany, 1993: (a) pp 9–29; (b) pp 1–8.
(63) Messiah, A. *Mécanique Quantique*; Dunod: Paris, 1972; Vol. 2; pp 447–456, 918–926.
(64) Blum, K. *Density Matrix Theory and Applications*; Plenum: London, 1981; pp 85–93.
(65) Ashcroft, N. W.; Mermin, N. D. *Solid State Physics*; Saunders: Philadelphia, 1976; pp 643–648.

$$\chi = \frac{M_{di}}{(1 - w_{mo})M_{di} + w_{mo}M_{mo}}[(1 - w_{mo})\chi_{di} + w_{mo}\chi_{mo}] \quad \text{(A11)}$$

Where χ_{di} and χ_{mo} are the powder susceptibilities of the Mn(III) dimer and monomer, respectively. This is the equation (1) used to calculate the susceptibilities of the dimer samples.

3. Interpretation of the Experimental Data. The magnetic susceptibilities of the monomer impurities among the dimer crystallites were assumed either to obey a simple Curie law

$$\chi_{Curie} = \frac{N_{Avog}g^2\mu_B{}^2}{3k_BT}S(S+1) \quad \text{(A12)}$$

with an isotropic factor $g = 2$ or to incorporate the effects of an axial ZFS Hamiltonian (A1) (see Discussion).

A direct orthonormal basis $\hat{i}, \hat{j}, \hat{k}$ of the molecular reference frame can be easily built from the crystallographic basis vectors $\vec{a}, \vec{b}, \vec{c}$ using the Schmidt orthogonalization procedure, i.e.

$$\hat{i} = \frac{\vec{a}}{a}, \quad \hat{j} = \frac{\vec{b} - \langle\hat{i}|\vec{b}\rangle\hat{i}}{||\vec{b} - \langle i|\vec{b}\rangle\hat{i}||}, \quad \hat{k} = \frac{\vec{c} - \langle\hat{i}|\vec{c}\rangle\hat{i} - \langle\hat{j}|\vec{c}\rangle\hat{j}}{||\vec{c} - \langle\hat{i}|\vec{c}\rangle\hat{i} - \langle\hat{j}|\vec{c}\rangle\hat{j}||} \quad \text{(A13)}$$

The basis vectors of both Mn(III) reference frames are simply defined from the positions of the four porphinato nitrogen atoms. For Mn(1) we choose

$$\hat{i}_1 = \frac{[1N(1) - 1N(3)]}{||[1N(1) - 1N(3)]||}, \quad \hat{j}_1 = \frac{[1N(4) - 1N(2)]}{||[1N(4) - 1N(2)]||},$$

$$\hat{k}_1 = \hat{i}_1 \times \hat{j}_1$$

where the 1N(l) are the coordinates of the l nitrogen around Mn(1) and the notation $[Q-P]$ represents the vector of origin P and end Q. Similarly, for Mn(2)

$$\hat{i}_2 = \frac{[2N(3) - 2N(1)]}{||[2N(3) - 2N(1)]||}, \quad \hat{j}_2 = \frac{[2N(2) - 2N(4)]}{||[2N(2) - 2N(4)]||},$$

$$\hat{k}_2 = \hat{i}_2 \times \hat{j}_2$$

The (Mn(2),$\hat{i}_2,\hat{j}_2,\hat{k}_2$) reference frame is nearly parallel to the molecular reference frame ($O,\hat{i},\hat{j},\hat{k}$) defined by eq A13, while the (Mn(1),$\hat{i}_1,\hat{j}_1,\hat{k}_1$) frame can be approximately obtained by a 180° rotation about the $\hat{j}$ direction, followed by a translation.

Analytical expressions of the magnetic susceptibilities can be found for unique magnetic centers with axial zero-field splitting[62a,66] or for symmetrical spin clusters with isotropic exchange interactions[67] when the single ion fine structure terms are neglected. On the other hand, for general spin clusters, numerical techniques should be employed although notable simplification occurs in the case of dominant exchange couplings.[68] Here, the various dimer susceptibilities are computed by diagonalizing the 25 × 25 matrices of the Hamiltonian $\mathcal{H}_{tot}$.

It is well-known[62a,66] that the influence of the ZFS anisotropy on the susceptibility of a unique magnetic center is most pronounced in the low-temperature region $K_BT/|D| \leq 5$. For the antiferromagnetic Mn(III) dimer samples, this is also the region where the susceptibility χ_{di} is expected to vanish while the monomer contribution χ_{mo} becomes dominant. Thus, the experimental data should be rather insensitive to the axial parameter D, which can be estimated only roughly. This will be discussed now in more detail. The axial ZFS effects for two identical spins $S_1 = S_2 = 2$, coupled by a rather strong antiferromagnetic interaction $J = -30$ cm^{-1}, are shown in Figure 9, where the parallel ($\chi_{||} = \chi_{zz}$), orthogonal ($\chi_\perp = \chi_{xx} = \chi_{yy}$), and powder susceptibilities (χ) are displayed as a function of temperature. The local frame of spin S_1 is taken to be exactly parallel to the molecular reference frame, while the local frame of spin S_2 is obtained through a 180° rotation about the $\hat{j}$ direction of the molecular frame. The axial parameters for both spins are $D = 10$ and -10 cm^{-1} in parts a and b, respectively, of Figure 9. This idealized situation nearly corresponds to that observed for our dimer. At low temperature, the parallel susceptibility $\chi_{||}$ is totally quenched by the antiferromagnetic coupling, while $\chi_\perp$ and χ become very small. Furthermore, as the axial parameter D changes sign, the $\chi_{||}$ and $\chi_\perp$ curves change side about the average values χ. This inversion of location of $\chi_{||}$ and $\chi_\perp$ leads to powder susceptibilities which are nearly insensitive to the sign of D. This unexpected effect was already observed for single Mn(III) centers in porphyrins[69] and emphasizes the necessity of single-crystal magnetic studies for an accurate determination of the sign and magnitude of D.

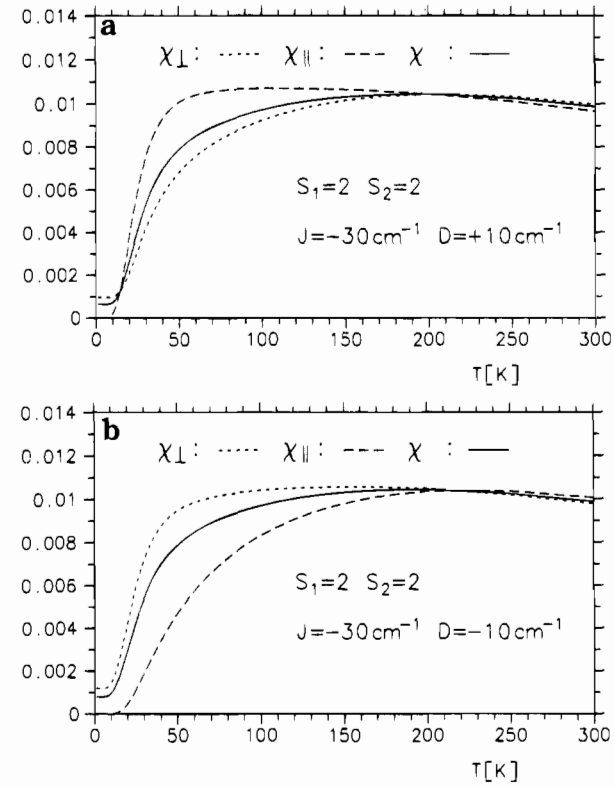

Figure 9. Theoretical temperature dependence of $\chi_\perp$, $\chi_{||}$, and χ for a binuclear complex with two identical spins $S_1 = S_2 = 2$ and an antiferromagnetic coupling $J = -30$ cm^{-1} in the idealized collinear Mn−O(H)−Mn geometry described in the Appendix, (a) with an axial zero-field splitting $D = +10$ cm^{-1} and (b) with $D = -10$ cm^{-1}. Note that with the above parameter set χ is nearly insensitive to the sign of D.

Supporting Information Available: Tables S1−S3, complete crystallographic details, anisotropic thermal parameters, and fixed hydrogen atom coordinates for {[Mn(OEP)]$_2$(OH)}ClO$_4$·3CH$_2$Cl$_2$; Tables S4−S6, those for [Mn(OEP)(H$_2$O)]ClO$_4$·H$_2$O; Table S7, complete structural results for [Mn(OEP)(H$_2$O)]ClO$_4$·H$_2$O; Table S8, magnetic susceptibility data for [Mn(OEP)(H$_2$O)]ClO$_4$·H$_2$O; Figure S9, an ORTEP drawing showing the porphyrin···porphyrin interaction for [Mn(OEP)(H$_2$O)]ClO$_4$·H$_2$O (13 pages). Ordering information is given on any current masthead page.

IC950678T

(66) Carlin, R. L. *Magnetochemistry*; Springer: Berlin, 1986.
(67) Belorizky, E.; Fries, P. H. *J. Chim. Phys.* **1993**, *90*, 1077.
(68) Fries, P. H.; Belorizky, E. *Nouv. J. Chim.* **1987**, *11*, 271. Belorizky, E.; Fries, P. H.; Gojon, E.; Latour, J. M. *Mol. Phys.* **1987**, *61*, 661.
(69) Behere, D. V.; Mitra, S. *Inorg. Chem.* **1980**, *19*, 992.